UTRECHT UNIVERSITY

Performance studies for the measurement of B^0 mesons in proton-proton collisions at 13 TeV with the ALICE experiment

by

Luuk Vermunt

Supervised by

dr. André Mischke

dr. Alessandro Grelli

in the

Faculty of Sciences

Institute for Subatomic Physics

January 2015

UTRECHT UNIVERSITY

Abstract

Faculty of Sciences
Institute for Subatomic Physics
by Luuk Vermunt

The Quark-Gluon Plasma (QGP) is predicted by Quantum Chromodynamics (QCD) to exist at extremely high temperatures and/or energy densities. In this state of matter, quarks and gluons are no longer confined to hadrons and behave asymptotically free. Near Geneva, at the Large Hadron Collider (LHC), experiments to study the properties of the QGP are performed. This thesis focuses on the measurement of beauty production in proton-proton collisions in the ALICE experiment (A Large Ion Collider Experiment), which is one of the four experiments at the LHC. Performance studies with Pythia Monte-Carlo simulations are done to investigate two B^0 meson decays. The new LHC centre-of-mass collision energy for proton-proton collisions (13 TeV) and the performance expected after the upgrade of the ALICE detector have been taken into account. This is done with realistic Monte-Carlo simulations, which describe the expected transverse momentum and pointing resolution for the upgraded Inner Tracking System (ITS) detector.

A hadronic and semi-leptonic decay of the B^0 meson are studied in this thesis, respectively $B^0 \to D^{*+} + \pi^-$ and $B^0 \to D^{*+} + e^- + \bar{\nu_e}$. The D^{*+} meson decays into $D^0 + \pi^+$ and the D^0 meson into $K^- + \pi^+$. The hadronic decay is relatively easy to reconstruct, however the branching ratio is quite low: $(3.04 \pm 0.4) \cdot 10^{-3}\%$. The semi-leptonic decay has a higher branching ratio (namely $(5.52 \pm 0.37) \cdot 10^{-2}\%$), but here a reconstruction procedure for the undetected neutrino is needed. This procedure is based on a recent analysis technique from the LHCb experiment. The yield extraction for both decays is performed by the invariant mass method for the expected number of events for Run-2. Unfortunately, due to limited statistics, this procedure worked only for the p_T integrated invariant mass distribution. Therefore, a counting procedure have been used for the six investigated transverse momentum intervals (0 - 3, 3 - 6, 6 - 10, 10 - 15, 15 - 20 and 20 - 30 GeV/c).

A study with the selection cuts used in this thesis becomes profitable for the hadronic decay channel at 35 billion events. At this number of events, the amount of B^0 meson decays will vary between 50 and 300 in all the p_T intervals. This leads to a statistical significance higher than 2.5, which means that it is possible to perform the invariant mass technique. A study into the semi-leptonic decay will be more difficult because the reconstruction method for the momentum of the neutrino broadens the width of the signal and shifts the peak position. This is unfortunate, because already at 3.5 billion events there will be approximately 200 B^0 meson decays, which pass the selection cuts in each p_T interval. The statistical significance will lie between 3 and 10, but due to the width of the peak and the background shape it is still difficult to fit the signal.

So both decays studied in this thesis look promising to study beauty production in real proton-proton collisions at $\sqrt{s} = 13$ TeV. However, a full AliRoot simulation is still needed to refine the results.

Introduction

In this thesis, the results of Monte-Carlo simulation studies on the measurement of B^0 mesons in proton-proton collisions at 13 TeV with the ALICE experiment are presented. By using dedicated Pythia simulations, tuned to reproduce real data, beauty production have been probed. The simulations use the upgraded centre-of-mass collision energy of the Large Hadron Collider (13 TeV for proton-proton collisions) and take the upgraded performance of the ALICE detector into account. The results obtained with this study are needed for the preparation for Run-2, which is expected to start in May 2015.

Two decay channels for the B^0 meson were studied. The first one consists of three decays via the hadronic decay channel. A beauty quark hadronize into a B^0 meson, which decays via $B^0 \rightarrow D^{*+} + \pi^-$. The D^{*+} decays as $D^{*+} \rightarrow D^0 + \pi^+$ and the D^0 meson in $D^0 \rightarrow K^- + \pi^+$. Before the start of this thesis, several studies into properties of this decay had already been done by the former bachelor student Daan Leermakers [1]. In this thesis, the focus will lie on the invariant mass analysis technique.

The second decay chain also includes a B^0 meson, which decays into a D^{*+} meson. Only this time, the decay is through the semi-leptonic channel: $B^0 \rightarrow D^{*+} + e^- + \bar{\nu_e}$. This decay has a branching ratio which is approximately 18 times higher than the first decay channel. However, the neutrino in this decay causes a problem because it can not be detected in the ALICE detector. So to properly study this decay, the missing momentum of the neutrino needs to be reconstructed. This have been done in a similar way as performed by the LHCb experiment [2]. Because this is the first study into this decay, the main purpose will be investigating if it is a profitable decay to study beauty production.

The simulations have been performed with the Monte-Carlo event generator Pythia 8. Pythia gives insight into the expected vacuum particle production, so the different resolutions of the ALICE detector need to be added in the model to reproduce real data. These resolution have been taken into account as well as possible to reflect the expected p_T and pointing resolution after the ITS upgrade. The reconstruction and yield extraction for both decays are performed by using the invariant mass technique. The results presented in this thesis, looks promising. However, a study with the AliRoot analysis framework is still needed to refine the results of this thesis.

Contents

Chapter 1

Subatomic physics

In the last decades there have been a lot of progress in the understanding of subatomic physics. Particle accelerators and detectors, like the Large Hadron Collider (LHC) and the ALICE experiment at CERN, have gone through immense developments resulting in new areas that could be explored. Another big development is the confirmation of the Standard Model by the discovery of proposed particles (for example the Higgs boson that was proposed by the Standard Model and discovered only a few years ago [3]). To give a chronological structure of the theory, and as a tribute for all the thousand physicists that contributed to the understanding of the subatomic world, this chapter will start with a brief history of subatomic physics.

1.1 Brief history

The first great thinkers that tried to explain the phenomenon matter were Greek philosophers. They came up with various theories, where the most proper was atomism conceived by Leucippus, Democritus and Epicurus. They made the outline for this philosophy which theorized that nature consists of two fundamental principles: atom and void. It means that matter can not be infinitely divided into smaller pieces, which is now known to be true. This theorem, that started philosophically, was taken up by physicists and chemists in the nineteenth century who did real instead of thought experiments. In this period more and more became known about molecules and atoms, what also increased the awareness that an atom could not be the smallest possible particle. This was confirmed by the discovery of radio-activity by Becquerel (1896), the electron by Thomson (1897) and the nuclei by Rutherford (1911). The exploration of the subatomic world could start and due to the upcoming quantum mechanics and special relativity it succeeded.

First, physicists became interested in the 'strong nuclei force', the force that holds the protons and neutrons in atoms together. The Japanese physicist Yukawa proposed a theory with a mediating particle, a meson. This particle, which he called a pion, mediates the force between the different nuclei and holds them together. The pion was discovered by Powel in 1947 and was a major breakthrough in particle physics. After its discovery the development of subatomic physics went fast. Due to collider experiments in 1950-1960, a lot of new particles were discovered. After this period, physicists were left with a whole zoo of particles but no clear scheme to organize them. The American

physicist Gell-Mann took this task upon himself and introduced the Eight-Fold way. This model sorted baryons and mesons in geometric patterns dependent on their charge and strangeness. The Eight-Fold way proposed new particles (for example Ω^-), which were soon to be found [4]. Understanding of the underlying physics came when Gell-Mann (and independently George Zweig) in 1964 hypothesised that hadrons are build out of even smaller particles, called quarks. He supposed that there were three flavours (up, down and strange), but a few years later a fourth and fifth quark were discovered (respectively charm and beauty). The discovery of the six and assumed last quark took longer because of its heavy mass. But 22 years after its prediction, this top quark was also found [5]. All the discoveries in the area of quarks and there binding forces are combined in a theory, which is called the Standard Model of particle physics. This overarching theoretical framework will be discussed in the next section.

1.2 The Standard Model

The Standard Model is the foundation of subatomic physics of the last decades. It describes all the elementary particles and fundamental forces which make up the matter around us. The elementary particles of this model are schematically illustrated in Figure 1.1. Since its finalizing in the 1970s discoveries of proposed particles, like the Higgs Boson, gave credits to this model. However, it is also known that the Standard Model falls short in certain areas. It can, for example, not give a complete theory, which contains all the four fundamental interactions.[1] The physics community is therefore trying to find theories outside the Standard Model like The Grand Unified Theory and Physics beyond the Standard Model.

The Standard Model describes three classes of fundamental particles: Fermions, Gauge Bosons and the Higgs Boson. A fermion is a particle with spin half-integer and a boson has spin integer. Fermions can be divided in two collections, leptons and quarks. There are six leptons (electron, muon, tau and their associated neutrinos) and six quarks (up, down, strange, charm, beauty and top). Each particle has an anti-particle which mass and spin is the same but with all the other quantum numbers opposite.

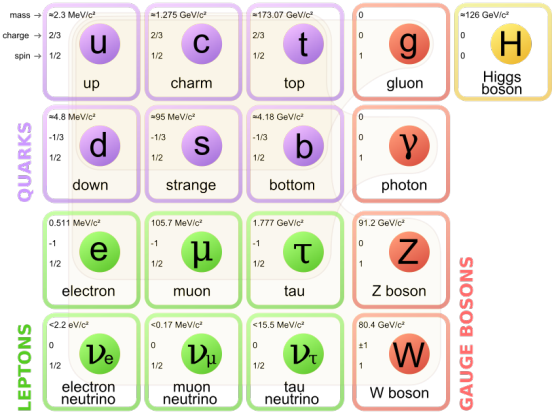

FIGURE 1.1: Standard Model of elementary particles: The 12 fundamental fermions, the 4 fundamental bosons and the Higgs Boson [7].

[1] The Standard Model can not explain gravity. It appears even to be incompatible with the most successful theory of gravity, general relativity [6].

Leptons are divided in three generations. These are made of respectively the electron and the electron neutrino, the muon and its neutrino, and the third generation consists of the tau and the tau neutrino. In contrast to quarks, leptons can exist independently from each other. However, only the electron is stable. The heavier muon and tau lepton will rapidly decay into an electron. Leptons are subject to three of the four fundamental interactions, namely gravitational, electromagnetic and the weak interaction. However, neutrinos are only affected by the weak-atomic force which is weak on the subatomic scale (hence the name). Because of this and its small mass, it is extremely hard to detect neutrinos and it took therefore a long time to discover them after their postulation by Pauli in 1930. Present-day, it is still a problem to detect a neutrino in particle detectors. The correction that has to be made to probe semi-leptonic decays (decays that includes a neutrino) will be discussed in detail in Chapter 5.

The six quarks can, just like the leptons, be divided in three generations. The first generation consists of the two lightest quarks (up and down), the second generation contains the strange and charm quark and the last generation is made out the two heaviest quarks: beauty and top. Ordinary matter is built from protons (uud) and neutrons (udd), so they only contain quarks from the first generation, which are stable. The top and beauty quarks occur only in extreme conditions: in particle accelerators or during the first milliseconds after the Big Bang. These six quarks and their anti-quarks build up the matter that are called hadrons. Hadrons can be two kind of particles, a meson (consists of a quark and an anti-quark) and a baryon (consists of three quarks or three anti-quarks).

However, this building out of quarks had one problem. Because quarks are fermions, and therefore have half-integer spin, they are subject to the Pauli Exclusion Principe. This quantum-mechanic principle says that two identical fermions can not occupy the same quantum state at the same time. So a proton, with two up quarks, could not exist. The solution came with the proposed colour charge by the American physicist Greenberg. This is a property of the quarks and is the strong interaction analog to charge in the electromagnetic interaction. Each quark was given a colour (red r, green g, blue b or their anti-colours anti-red $\bar{r}$, anti-green $\bar{g}$ or anti-blue $\bar{b}$). A bound state of quarks, like a hadron, had to be colourless or colour-neutral. This colour charge allows three quarks to coexist and satisfy the Pauli Exclusion Principle.

The force between quarks is called strong force (or colour force) and is the fundamental interaction, which is understand the least. The strong force does not drop off with distance and is about 137 times stronger than the electromagnetic force. This force is responsible for the confinement of quarks. It involves the exchange of gluons and is so strong that quark-anti quark production happens before quarks can separate.

Three of the four fundamental forces are incorporated in the Standard Model. The Standard Model, however, does not give an explanation for the fourth force, gravitation. A force is transferred by a force carrier, also known as gauge boson (see fourth column in Figure 1.1). The gluon carries the strong force, the electromagnetic force is transferred by photons (static or virtual) and the weak interaction makes use of Z and W bosons.

In this research, we are interested in the Quark-Gluon Plasma, which is hypothesized to exist at extremely high density or temperature. It is believed that the Universe was in this state a few milliseconds after the Big Bang. This phase is dominated by the strong interaction, so in the next section the theory that describes this strong force, Quantum Chromodynamics, will be discussed.

1.3 Quantum Chromodynamics

Quantum Chromodynamics (QCD) is the theory that describes the interaction between quarks and gluons. This interaction is working on the colour charge of these particles. Not only quarks, but also gluons, carry colour (gluons are a mixture of a colour and an anti-colour). This makes Quantum Chromodynamics hard to understand because its mediators, gluons, are also participating in the strong interaction. There are nine colour combinations for gluons, but there exist only eight types of gluons in QCD. This is because the linear combination $r\bar{r} + b\bar{b} + g\bar{g}$ must be non-interacting. Otherwise colourless baryons would be able to emit these gluons and interact with other colourless baryons. This is not observed in experiments.

Because of gluons carrying colour, they can interact with other gluons. These gluon-gluon interactions make up a colour field which confines the quarks into hadrons. This field does, in contrast to the electromagnetic force, not decrease when the distance between the quarks is increased. When quarks are separated, the interaction of the gluons themselves will cause the colour field lines to bunch together, which increases the energy stored in the field. At large enough distance, about 10^{-15} meter, the energy threshold is reached and increasing the distance will merely cause a new quark-anti quark pair to form (Figure 1.2). Another way of gluons interacting with themselves are glueballs. These are particles that consist solely of gluons and are therefore extremely difficult to detect. There are, however, strong suggestions that a particle what could be a glueball have been found [8].

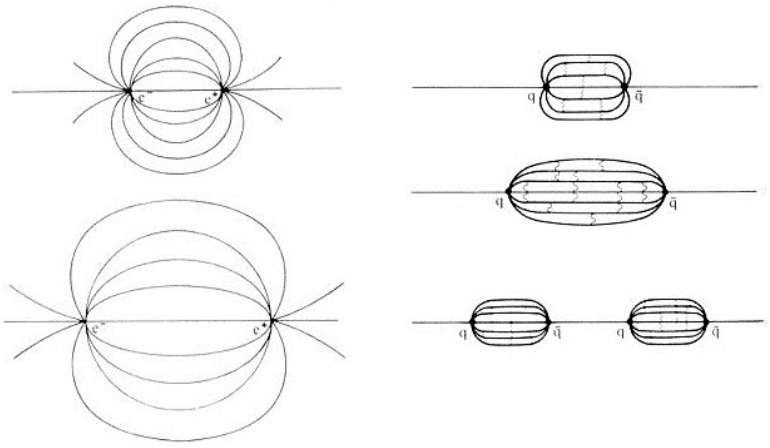

FIGURE 1.2: Difference between field lines in QED (left) and QCD (right) when the distance between particles is increased. At a certain distance the energy threshold for QCD is reached and a new quark-anti quark pair are formed [9].

Like Quantum Electrodynamics (QED), QCD can also be written in terms of a potential. For the short-distance one-gluon exchange force between two heavy quarks, this potential can be approximated by a coulomb-potential with an added confinement term:

$$V(r) = -\frac{\alpha_s k}{r} + Ar. \tag{1.1}$$

The coupling constant α_s is the strong force analogy of the fine structure constant from QED, characterizing the strength of the interaction. It is defined in the following way,

where μ is the renormalization mass, q the four-momentum transfer and n_f the number of flavours

$$\alpha_s(q^2) = \frac{\alpha_s(\mu^2 c^2)}{1 + \frac{\alpha_s(\mu^2 c^2)}{12\pi}(33 - 2n_f)\ln\frac{q^2}{\mu^2 c^2}}. \tag{1.2}$$

So the structure constant in QCD is dependent on the exchanged four momentum. This means that at large distances α_s is large and for short distances it is small. The fine structure constant in QED also changes with momentum but much more slowly and in the other direction (becomes slightly larger at high momentum). So quarks act like free particles in a hadron and therefore perturbation theory can be performed. This results in the prediction of a phase transition for $\alpha_s \ll 1$. Hadrons change into a state where quarks and gluons can exist freely, which is called asymptotic freedom. This state of matter is the Quark-Gluon Plasma (QGP) and of great interest for the physics community.

1.4 Quark-Gluon Plasma

The QGP is a phase hypothesized by QCD where quarks and gluons are asymptotically free. In this phase, quarks and gluons are no longer confined into hadrons, but can move around in a bigger volume. It is believed to exist at extremely high temperatures, density or both. The early Universe, a few milliseconds after the Big Bang, is assumed to have been in this state. So when physicists reach a point where they understand the properties of the QGP, a big step in understanding this part of the expansion of our Universe is accomplished too. Because of this, research into the Quark-Gluon Plasma is highly regarded. As indicated in the phase diagram in Figure 1.3 there are already two particle colliders that can produce high enough energy to form a Quark-Gluon Plasma. These are the Relativistic Heavy Ion Collider (RHIC) in the USA and the Large Hadron Collider (LHC) in Switzerland.

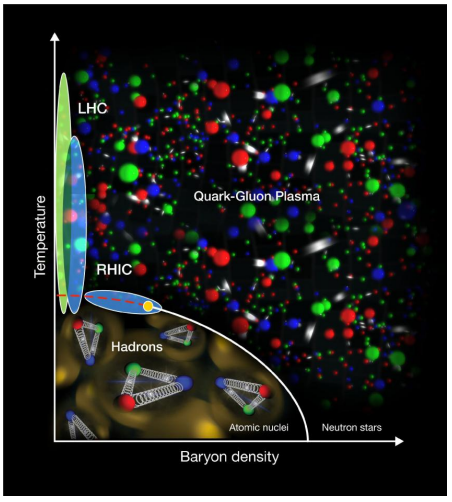

FIGURE 1.3: The phase diagram for QCD matter resulting in hypothesizing a Quark-Gluon Plasma at extremely high temperatures or density [10].

RHIC can produce a Quark-Gluon Plasma in multiple energy ranges, but it takes only moments before the matter cools down to its normal state. The LHC is able to produce QGP which lasts longer. Currently, the LHC is getting ready for its second three-year run which is expected to start in May 2015. Since 2010 the LHC was running at a centre-of-mass collision energy of 7 TeV for proton-proton collisions and 2.76 TeV for lead-lead collisions. The second-run is planned to run at an energy of 13 TeV for proton-proton reactions and 5.1 TeV for lead-lead collisions.

At the LHC, the QGP is produced by colliding two energetic lead ions. Due to the high velocity these ions have, relativistic length contradiction reshapes them into two disks. The overlap between these disks during the collision is called centrality. A centrality of zero means the ions collide head-on and a centrality of 100 percent indicates the minimal overlapping region. In Figure 1.4 a head-on collision of two gold nuclei is schematically described. In stage [c] the matter is in a Quark-Gluon Plasma phase.

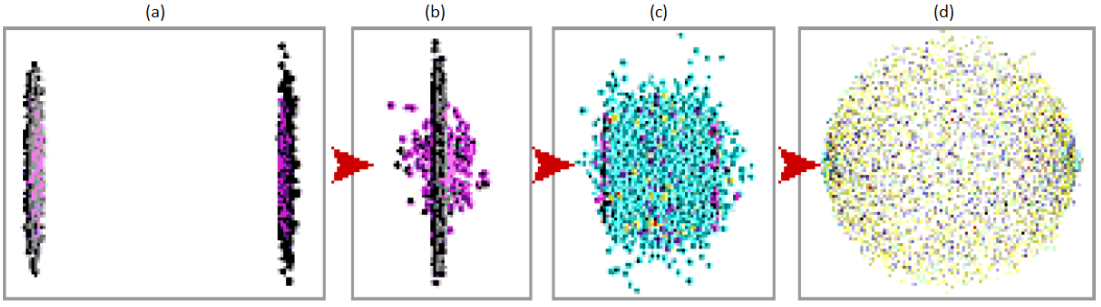

FIGURE 1.4: Different stages during a head-on collision of two heavy ions. When the two nuclei collide [a], some of the energy is transformed into intense heat and new particles [b]. Heavy quarks are produced in this stage. When the conditions are right a Quark-Gluon Plasma can be formed [c] after which the quarks will become confined in hadrons again [d] [11].

Because of the short lifetime, it is impossible to observe the QGP directly. The quarks and gluons have been hadronised before they can reach the detector. But through a reconstruction of the detected particles, the properties of the QGP can be retrieved.[2] Interesting decay chains to study QGP are the ones that contain heavy quarks like charm and beauty. As shown in stage [b] in Figure 1.4, heavy quarks are produced in the early stages of the collision and therefore travel through the developing QGP. This forms an interesting probe to study properties of the QGP. In the next section, the production of these heavy flavour quarks and their relation with the QGP will be discussed in more detail.

1.5 Heavy flavour production

In a collision of two nuclei, heavy quarks can be produced together with the Quark-Gluon Plasma. There are mainly two ways to produce heavy quarks. Two gluons that collide can produce a heavy quark-anti quark pair with their shared energy or a quark can annihilate with its anti quark and produce a heavier quark and anti quark. The production time of quarks is about $1/2m_q$, so the heavy quarks, like charm, beauty and

[2]For a proton-proton collision at 13 TeV the number of final particles will already be from the order $\mathcal{O}(10^2)$. These detected particles are mainly pions, kaons, protons and electrons.

top, will be produced before the Quark-Gluon Plasma is formed. This means that they travel through the QGP and lose energy due to interactions with the plasma.

The way quarks lose energy to the plasma is similar to an electron which loses energy by radiating Bremsstrahlung. Electrons radiate photons when they travel through matter, quarks lose their energy by radiating gluons. This energy loss is smaller for heavier quarks due to the dead cone effect. When the radiation angle is small compared to the mass, $\theta < m_q/E_q$, gluon radiation will be suppressed [12]. Because of this lower energy loss for heavy quarks, its mesons are more likely to be seen sufficiently far away from the collision point. This is another reason why heavy flavour production is interesting to study the QGP. From the three heaviest quarks the top quark has the shortest decay time, so it will decay before it can form top mesons. However, charm and beauty quarks live long enough to travel through the QGP and hadronisate afterwards. These quarks, and therefore also their mesons, contain information about the full development of the Quark-Gluon Plasma.

The properties of the mesons produced by these heavy quarks need to be compared with information about the same decay channel but without the QGP. This is done by colliding two protons instead of colliding lead ions. Protons contain only one nucleus instead of the 207 nuclei for lead ions. In such a proton-proton collision, heavy quarks are produced but no Quark-Gluon Plasma is formed. So the mesons from these proton-proton collisions can be compared with the ones that traveled through the QGP. The differences give important information about the properties of the QGP.

Chapter 2

Experimental setup

CERN, the Europeon Organization for Nuclear Research located near Geneva, is one of worldwide most respected centers of scientific research. Here, physicists are doing research on the fundamental principles of our Universe. This is done by colliding nuclei with high energies and detect the outcoming particle production. Currently, there are running different experiments at CERN, of which one of them is the ALICE experiment (abbreviation for A Large Ion Collider Experiment). The ALICE detector is a heavy ion detector at the LHC. This Large Hadron Collider is world's largest and most powerful particle accelerator. In this thesis, the focus will lie on the ALICE experiment, but this is not the only experiment at CERN. Three other big experiments at the LHC are the ATLAS, LHCb and CMS experiment.

2.1 The ALICE detector

ALICE is the dedicated heavy-ion detector and is designed to study lead-lead collisions at a maximal centre-of-mass energy of 5.5 TeV per nucleon-nucleon pair. At this energy, the lead-lead collisions will form a Quark-Gluon Plasma which is the main research topic of the ALICE Collaboration. After more than three years of successful operation, the ALICE detector is currently being upgraded. The 17 of the existing ALICE sub-detectors will be improved and the new DCAL detector (abbreviation for Dijet Calorimeter) is installed.

The ALICE detector is schematically shown in Figure 2.1. It consists roughly of two parts: The central barrel and the forward muon spectrometer. The central barrel is the part where this research will focus on. This part of the detector measures the hadronic signals produced by the collision. However, not all of the produced hadrons can be measured. This is because the ALICE detector has a coverage in pseudo-rapidity ($|\eta| < 0.9$). The pseudo-rapidity coordinate describes the angle of the particle relative with the beam axis and is preferred over the polar angle θ because differs in η are Lorentz invariant. $|\eta| < 0.9$ corresponds with a polar angle between 0 and 45 degrees in both directions. In contrast to the polar angle, the full azimuthal angle is covered. The second part of the ALICE detector, the forward muon spectrometer, is dedicated to study flavour-hidden mesons build out of a quark and its own anti-quark (for example the J/Ψ meson, which is a $c\bar{c}$ state). This part of the detector is not interesting for this thesis so will not be explained further.

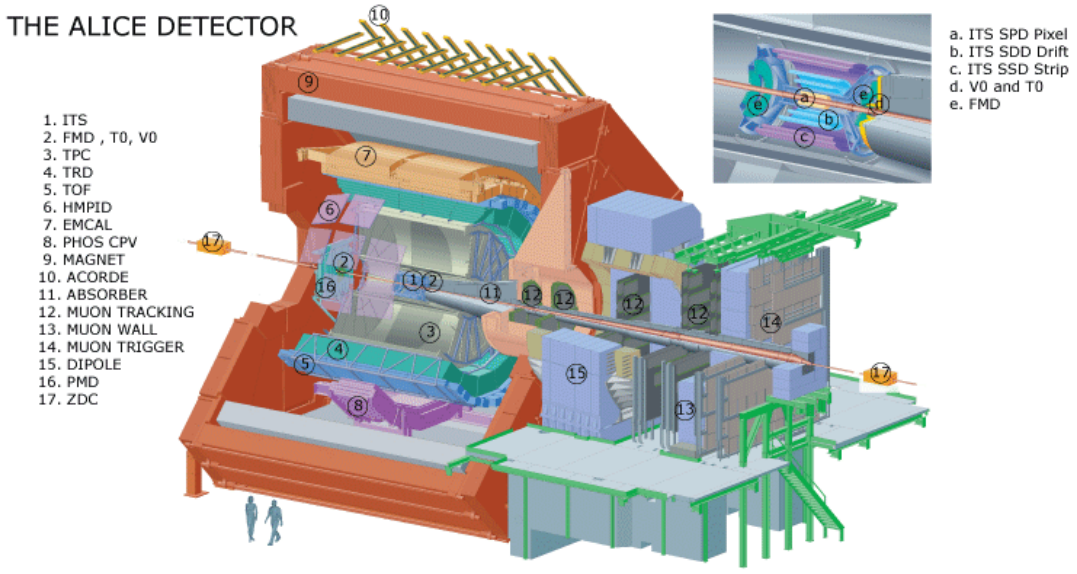

FIGURE 2.1: A schematic view of the ALICE detector with its 17 subdetectors [13].

An ensemble of cylindrical detectors, that surround the interaction point, is used to track all the particles that are emitted from the Quark-Gluon Plasma. The ITS, the TPC and the TRD detector measure the passage of each charged particle for different points and give so precise information about the particle's trajectory. All these tracking detectors are embedded in a large magnet (with a magnetic field strength of 0.5 Tesla), which bends the trajectories of the charged particles. From this curvature the momentum can be determined. In the remainder of this section the, for this research, most important sub-detectors will be explained in more detail. These are the vertexing, tracking and particle identification detectors ITS, TPC and TOF.

2.1.1 Inner Tracking System

The Inner Tracking System (ITS) is a cylindrically-shaped silicon detector closest to the interaction point and is important to distinguish between 'prompt' particles and particles generated by the decay of short-living particles.[1] It measures the primary and secondary vertices (the points of formation and decay) of the fast decaying particles for distances as small as 0.1 millimeter. The B^0 meson decay chains, that are the topic of this thesis, have short lifetimes (approximately 10^{-12} seconds), so the ITS detector is of great importance to measure their vertices.

The ITS consists of six layers of silicon detectors located at radii between 3.9 and 43 cm from the beamline (see Figure 2.2). Silicon detectors work by doping strips of silicon (bringing in impurities) to turn them into diodes. When a charged particle pass through such a strip, it causes a small ionization current that can be detected and measured. Thousand of these strips can yield an accurate picture of the path the particle took. The two innermost layers contain Silicon Pixel Detectors (SPD), for the two intermediate layers Silicon Drift Detectors (SDD) are used and the two outermost layers are equipped with Silicon Strip Detectors (SSD). The layers cover different pseudo-rapidity ranges, but the whole ITS detector has the same $|\eta| < 0.9$ coverage as the ALICE detector.

[1] Prompt particles are particles that are produced during the collision.

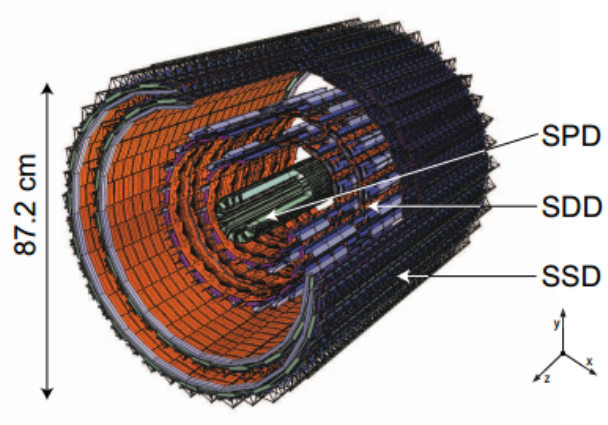

FIGURE 2.2: The Inner Tracking System (ITS detector) schematically shown with its three different layers (SPD, SDD and SSD) [14].

The design of the current ITS detector is optimized for track finding and displaced vertex reconstruction. However, there are several frontiers for which the current experimental setup is not yet fully optimized. Besides, the improved luminosity for Run-2 will demand more from the ITS. ALICE is therefore planning an upgrade for the ITS detector for Run-3 in 2018-2019 [15]. For example, a movement of the first layer closer to the beam line, to improve the measurement of the impact parameter, will be implemented. Information about the expected performance for the upgraded ITS detector have been taken into account in the simulations performed in this thesis.

2.1.2 Time Projection Chamber

The Time Projection Chamber (TPC), schematically shown in Figure 2.3, is a gas detector filled with a Ne/CO_2 gas mixture (90 : 10). It surrounds the ITS and operates as the main tracking device of the ALICE detector. TPC detectors have large solid angles, have great spatial resolution in three dimensions, allow good pattern recognition and generate charge and mass information of the particles. This is accomplished by an electric field inside the TPC, with a strength of 400 V/m. A charged particle that travel through the chamber produces ion pairs along its trajectory. The removed electrons are accelerated to the end of the chamber by this electric field. The point of impact of the electrons traces the projection of the particle trajectory.

The TPC in the ALICE detector covers the full azimuthal angle and has a $|\eta| < 0.9$ pseudo-rapidity coverage. It has an inner radius of 84.1 cm, an outer radius of 246.6 cm and a 88 m^3 active volume filled with gas. The main functions of the TPC are track finding and track separation, but it is also capable of charged particle momentum measurement and particle identification. This is done by measuring the particular energy loss (dE/dx) for the particles. The amount of lost energy per distance for a given momentum can identify the particles (see Figure 2.4).

2.1.3 Time Of Flight detector

Further particle identification is performed by the Time Of Flight Detector (TOF). This detector is optimized for charged particles in the intermediate momentum range (below

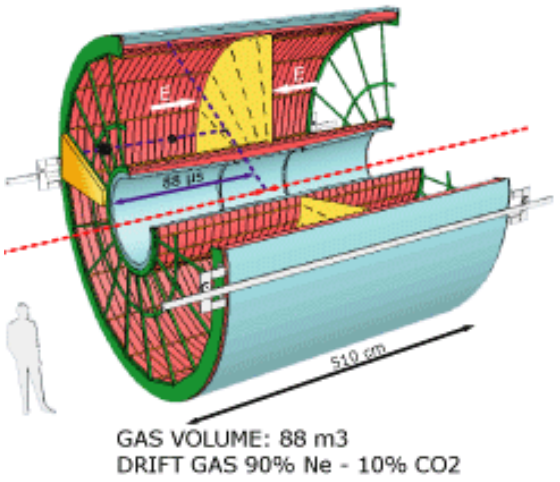

FIGURE 2.3: Schematic view of the Time Projection Chamber (TPC detector) [16].

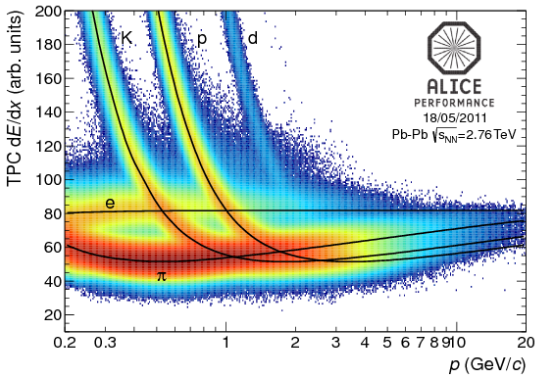

FIGURE 2.4: Particle identification performed by measuring $\mathrm{d}E/\mathrm{d}x$ in the Time Projection Chamber. The curves show the $<\mathrm{d}E/\mathrm{d}x>$ for π, K, p and e [17].

2.5 GeV/c). It can discriminate two particles with different mass but same momentum using the time of flight. This is the time that a particle needs to pass the gaps between two scintillators. This is compared with the expected value, which depends on the particles mass hypothesis computed from its track length and momentum, to identify the particle.

The TOF has a cylindrical shape and covers the angles between 45 and 135 degrees, so has a pseudo-rapidity range of $|\eta| < 0.9$. Like the ITS and TPC the full azimuthal angle is covered. It consists of 157.248 readout pads divided over 1638 MRPC strips making up a 160 m^2 active surface. In Figure 2.5 a schematic overview of the technical design for the TOF detector is shown.

The time resolution for the TOF is better than 100 ps which provide 3σ separation up to 2.2 GeV/c for pion/kaon and up to 4 GeV/c for kaon/proton (see Figure 2.6). The time of flight measured by TOF is combined with the results from the ITS and TPC for final particle identification. This combining has proved to be useful in improving the separation between different particle types.

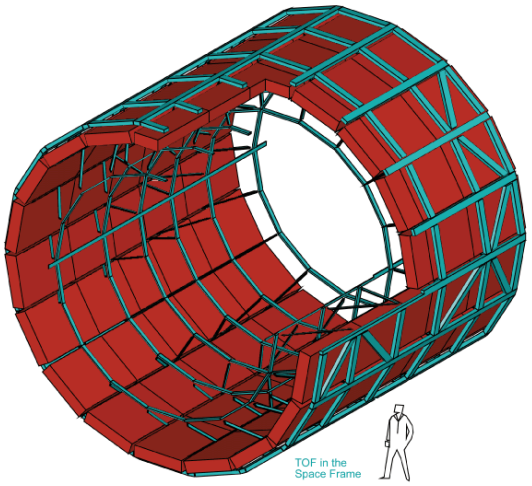

FIGURE 2.5: A schematic image of the Time Of Flight detector inside the ALICE detector [18].

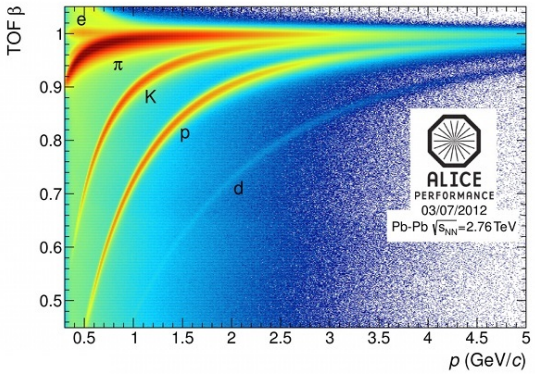

FIGURE 2.6: Particle identification performed by measuring the particles velocity β in the Time Of Flight detector. The bands for electrons, pions, kaons and protons are clearly visible [19].

2.2 The Analysis framework

Different simulation and analysis methods have been used during this thesis. Event generator Pythia is used to simulate proton-proton collisions and the analysis of the Monte-Carlo data is done with the ALICE Root/AliRoot framework. These will be discussed shortly in the following subsections.

2.2.1 Root

Root is an object-oriented data analysis framework written in C++, originally designed by René Brun and Fons Rademakers in 1995. Nowadays, it is used by thousand of physicists in different areas all over the world. The backbone of Root is a layered hierarchy with classes, libraries and modules. Currently, there are around 1200 classes, grouped in 60 libraries, which are divided in 19 modules. Most of the classes are connected with

a common base class *TObject*. This give the opportunity of direct access to the separate attributes of the selected data. Users can interact on different ways with the Root software: via command line, batch script or via a graphical interface [20].

In this thesis, Root is mostly used to process and plot the produced Monte-Carlo data. Properties of the produced particles are stored in histogram classes, like *TH1F*. These histograms can be in 1D, 2D or 3D and provide many different plot options. Another Root category that have been used multiple times is the minimization category that provides classes with Minuit, Fumili and linear fitter algorithms. These classes have been used to fit the produced data.

2.2.2 Pythia

For this thesis, the data is obtained with simulations performed by PYTHIA 8.1.86. The Pythia program is a tool for the generation of high-energy collisions using a coherent set of physical models to calculate the evolution of the system.

Pythia is a Monte-Carlo event generator which generates complex sets of hadronic outgoing particles from a few-body hard process like a proton-proton collision. Pythia is focused on centre-of-mass energies greater than 10 GeV. The code package contains a library with the laws of Quantum Chromodynamics and models for different events like initial- and final-state parton showers, multiple parton-parton interactions or particle decays. Pythia 8 is the first version that is fully written in C++, previous versions were using Fortran.

Event generators are used mainly for two kind of studies. Firstly, results obtained with Monte-Carlo simulations can be compared with existing data to extract physics. In Pythia, everything is precisely known, so a particular event can be traced back to its source. Another possibility with event generators is to study physics at future experiments, so what can be expected. This is what have been done in this thesis for the new LHC centre-of-mass collision energy and the upgraded performance of the ALICE detector.

The physics topics in Pythia 8 can, roughly, be divided in three stages [21].

1. The generation of a process, calculated with perturbation theory, that decides what the nature of the event is. For example the 'hard process' that was used in these simulations: $q\bar{q} \to b\bar{b}$ or $gg \to b\bar{b}$. So in every event a beauty and anti-beauty quark have to be produced. This is called beauty forced.

2. The generation of all activity on quark level. For example initial- and final-state showers or multiple quark-quark interactions. A realistic quark structure has been obtained at the end of this step.

3. The hadronization of the quark configuration by string fragmentation. This is a parton fragmentation model that explains many features of the hadronization process quite well. After this step unstable particles decay, what results in realistic events, that could be observed in the real world.

Each step calls on a different class, respectively ProcessLevel, PartonLevel and HadronLevel. Each of these levels contain classes that can perform different kinds of physics

tasks. The information between these three classes flows mostly by the Event Class. This class contains the full story from the incoming beams to the final hadrons, using a large vector filled with the produced particles and their properties. These properties can be retrieved by using member functions. For example the transverse momentum of a particle can be obtained by the event.pT() method. These properties are stored using histogram classes from the Root framework.

Pythia does not include the interaction between particles and detector, it calculates the vacuum particle production. So when physicists want to compare real data with Pythia Monte-Carlo data, the interaction between particles and detectors have to be added in the model. A transport code, like Geant, provides the opportunity to take these interactions into account.

2.2.3 AliRoot

Where in this thesis Root is used to analyse data, the actual ALICE offline analysis framework is performed by AliRoot. AliRoot is based on Root and can handle data from Monte-Carlo simulations and actual collision data obtained with the ALICE detector. It can produce its own Monte-Carlo simulation as well, where the interaction between particles and detector is included using the toolkit Geant [22].

AliRoot is designed in different layers [23]. In the first layer an event generator is loaded (Pythia or HIJING). These event generators produce, using Monte-Carlo techniques, a list of final particles with their corresponding properties. Pythia works the same as described in the previous section. In the second layer the ALICE detector itself comes into view. AliRoot contains the full construction of the detector and the specific heat loss per material. A transport code, like Geant, simulates the interactions between particles and these different kind of matter. Each particle is tracked till it leaves the full ALICE detector or does not have any measurable energy left. In this second layer, the physical processes like decays can also happen.

The next layer quantizes the responses of the ALICE detector on its interactions with particles. Each particle, with enough energy, that travel through an active part of the detector corresponds with a hit. All these hits are stored in files. These, enormous, data files looks almost the same as data obtained during a real collision. So from this point on the different kind of data, Monte-Carlo or real, are handled the same. Algorithms look for clusters of hits and reconstruct the tracks and other properties of the particles. All this information is stored in a file where users can extract information with their own macros. Because of the enormous size of these data files this analysis is normally done on the Worldwide LHC Computing Grid (WLCG). This is a global collaboration of more than 170 computing centres in 40 countries [24].

Chapter 3

Pythia Monte-Carlo simulations

In this thesis, two different decay chains of the B^0 meson have been studied. The probability of finding one of these two decay chains in a proton-proton collision is very low. Only in 1.5 percent of the collisions a beauty quark is created. There will also be a probability to form the B^0 meson out of this beauty quark and for the B^0 meson to decay through one specific decay channel. In particle physics, this probability is called the branching ratio of the decay. For example, the branching ratio for a B^0 meson to decay in $D^{*+} + e^- + \bar{\nu_e}$ is $(4.93 \pm 0.11)\%$ and in $D^{*+} + \pi^-$ it is only $(0.276 \pm 0.013)\%$ [25]. So to reconstruct the properties of the B^0 meson to study beauty production, a lot of collisions are needed to get sufficient statistics.

The data is obtained with Pythia Monte-Carlo simulations. To speed up this process a special configuration in Pythia can be used. This is called beauty forced, which means that in every collision a beauty and anti-beauty quark are forced to be produced. Beauty forced is one of the two setups that have been used in this thesis. The second one is called minimum bias, which describes reality as good as possible.

The data obtained with these two configuration files have to be checked on verity. In this chapter, the used configuration types and the performed checks on the model will be discussed. In the last section, a first, but fundamental, procedure towards producing data that looks like real data is explained. This procedure is called smearing of the transverse momentum.

3.1 Configuration types

Pythia makes use of the Monte-Carlo technique. Such a Monte-Carlo simulation rely on repeated random sampling to simulate data for a given mathematical model. In the case of Pythia, this model is build out of the laws of Quantum Chromodynamics described by the string fragmentation model. The randomness in the behaviour of particles, that is introduced because of quantum mechanics, can be simulated using these Monte-Carlo techniques. In Pythia, different methods of producing random, uncorrelated numbers are used, but an explanation of these methods is outside the scope of this thesis. A detailed description can be found in [26].

There are a lot of configuration options inside a Pythia Monte-Carlo simulation that give users the possibility to generate specific events. Two of them are used in this thesis. As

said before, the investigated events have a small probability to occur in a proton-proton collision. So, to investigate the signal, Pythia is configured in a way called beauty forced (shown below).[1] The first two rows indicate that in every event a beauty pair have to be produced.

- HardQCD:gg2bbbar = on,
- HardQCD:qqbar2bbbar = on,
- BeamRemnants:primordialKT = on,
- BeamRemnants:primordialKTsoft = 0,
- BeamRemnants:primordialKThard = 2.03,
- BeamRemnants:halfScaleForKT = 0,
- BeamRemnants:halfMassForKT = 0.

To perform the invariant mass technique or to calculate the effectiveness of applied cuts, studies into the background distributions for these decays are needed.[2] These background studies have to describe the reality as well as possible, so forcing the production of beauty quarks is not an option. Therefore, another configuration is used, called minimum bias (shown below). This configuration produces events that look quite similar to the collisions, which can be observed in the ALICE detector.

- SoftQCD:all = on,
- PartonLevel:MI = on,
- MultipleInteractions:pTmin = 1.9,
- MultipleInteractions:pT0Ref = 1.8,
- MultipleInteractions:ecmRef = 1000,
- MultipleInteractions:expPow = 0.16,
- MultipleInteractions:bProfile = 2,
- MultipleInteractions:coreFraction = 0.16,
- MultipleInteractions:coreRadius = 0.5,
- SigmaProcess:factorMultFac = 1.

In this thesis, all simulations have been done using the expected LHC centre-of-mass collision energy for proton-proton collisions of 13 TeV, except if explicitly stated otherwise.

3.2 Performed tests on verity

Before the Monte-Carlo data can be analysed, tests on verity of the model are needed. Normally, a lot of checks are performed before the simulated data will be accepted, but that falls outside the scope of this thesis. Therefore only a few tests are described in this chapter.

[1] A signal event is a collision that produces one of the investigated decay chains of the B^0 meson.

[2] A background event is a collision where the reconstruction procedure on some random tracks leads to a potential B^0 meson.

Up to now there are no bugs found in Pythia 8.1.86, so it is likely that it describes QCD correctly. To confirm this, results from Pythia are compared with other calculation methods. Interesting values like the branching ratio of the investigated decays or the lifetime of a particle need to be checked too. Because of the large amount of particles and the still continuing research these values could be out of date, which is interesting to know because it could effect the results. These checks are described in the next sections.

3.2.1 FONLL calculations

The minimum bias configuration have to describe reality as good as possible. Therefore, it is interesting to compare results obtained with Pythia with a different calculation method, which is known to be more precise in describing QCD. For this purpose, the p_T distribution from Pythia is compared with calculations done with the FONLL framework. FONLL stands for Fixed Order plus Next-to-Leading Logarithm and is a program that calculates the transverse momentum and rapidity distributions for heavy quarks in hadron-hadron and photon-hadron collisions. The accuracy of the FONLL calculation can be denoted as being FO+NLO+NLL (so it is accurate to the leading order (LO), next-to-leading order (NLO) and next-to-leading logarithms terms (NLL)) [27, 28]. Pythia itself uses perturbative QCD calculations, which are only exact at LO. Some of the NLO processes like pair creation, flavour excitation and gluon splitting are included in Pythia but these are not all of the next-to-leading order terms. The comparison with FONLL will give information about the lack of the missing processes. For the FONLL calculation framework, the following settings are used:

- FONLL v.1.3.2. [$\mathrm{d}\sigma/\mathrm{d}p_T^2\mathrm{d}y$ (pb/GeV^2)],
- quark = bottom,
- final state = Dstar from a single B. NP params (cm, lm, hm) = 24.2, 26.7, 27.2,
- BR(q $\rightarrow$ meson) = 1,
- BR(B $\rightarrow$ Dstar) = 0.173,
- PDF set = CTEQ6.6,
- ebeam1 = 7000, ebeam2 = 7000 (this is for 14 TeV),
- ptmin = 0,
- ptmax = 30,
- etamin = -0.9,
- etamax = 0.9,
- cross section is $\mathrm{d}\sigma/\mathrm{d}p_T$ (pb/GeV).

As can be seen in Figure 3.1, the ratio of the p_T distribution from the D^* meson at 14 TeV and 7 TeV from Pythia corresponds very well with the ratio distribution of differential cross section for $b \rightarrow B \rightarrow D^*$ obtained with FONLL calculations.[3] Almost all the blue points lie inside the error band. However, the central value of the single distributions itself, differ a bit. From these plots it can be concluded that Pythia produces softer beauty quarks at both energies than in a real collision.

The comparison with the FONLL calculation framework is performed using the minimum bias configuration, but the signal events are produced using beauty forced. So the

[3] At 3 December 2014, there was an update, which implemented the option 13 TeV in the FONLL calculation framework. This was, unfortunately, too late for this thesis.

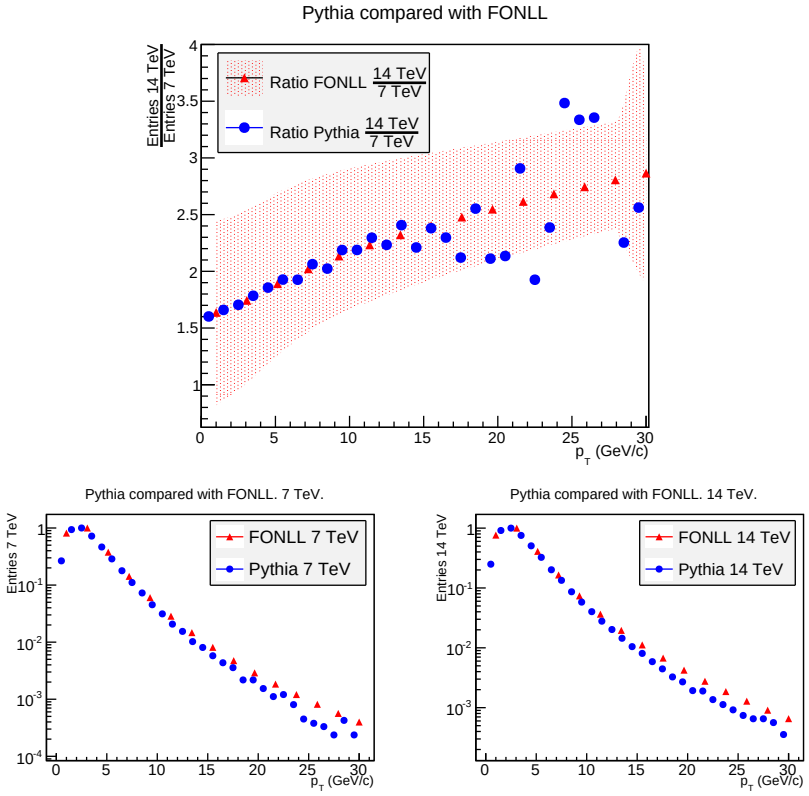

FIGURE 3.1: A comparison between the p_T distribution of D^* mesons coming from $b \to B^0 \to D^*$ (Pythia) and the differential cross section for this decay (FONLL). The blue dots are the results obtained with Pythia simulations and the red dots are obtained with calculations using the FONLL framework. The top plot shows the ratio for 14 TeV divided by 7 TeV. The two lower plots show the single distributions for these two energies.

difference between properties of the B^0 mesons using beauty forced and minimum bias configuration is also an important check. The transverse momentum distributions of these two types of configuration are compared, which can be seen in Figure 3.2. The two distributions look very similar but are not quite the same. The transverse momentum for minimum bias is shifted toward higher values. Or in other words, the beauty forced distribution provide us with even softer B^0 mesons. For the studies done in this thesis, the small differences between FONLL, minimum bias and beauty forced will not have a large effect on the results and therefore it will be assumed that both configurations produce the correct distribution of beauty quarks.

3.2.2 Properties of the B^0 meson

Another necessary check is to compare the values that are specific for a B^0 meson, like the branching ratio or lifetime, with the assumed correct value from the Particle Data Group. In Figure 3.3, the calculated branching ratios for the investigated B^0 decays are plotted on top of the real value. The probability for a B^0 meson to decay via $B^0 \to D^{*+} + e^- + \bar{\nu}_e$ is in Pythia about 14% too high. Note, that this percentage have

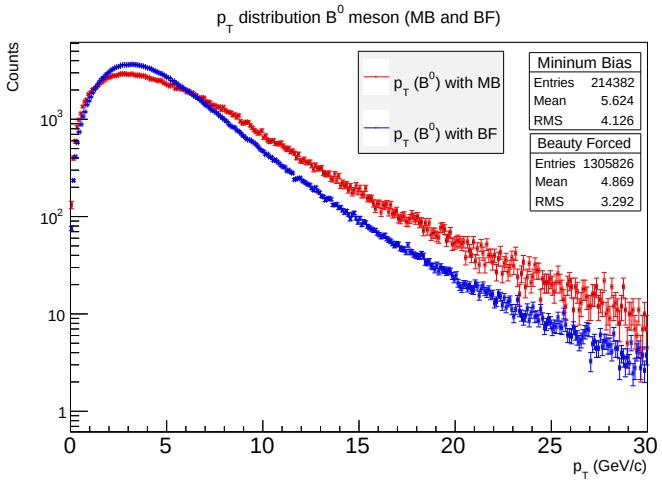

FIGURE 3.2: p_T distribution for B^0 mesons using the minimum bias (red symbols) and beauty forced (blue symbols) configuration.

not been taken into account for the results presented in Chapter 5 and Appendix B. The other branching ratios in Pythia correspond with reality.

Another interesting fact that can be read from Figure 3.3 is that in 75% of the events the B^0 meson has a B^{*0} as mother. A B^{*0} meson has a very short lifetime and decays always in $B^0 + \gamma$. Because of this short lifetime the decay vertex of the B^{*0} meson can not be distinguished from the collision point and so the daughter B^0 meson will look the same as a prompt B^0. Therefore, both productions of a B^0 meson are taken into account in this thesis.

Because cuts will be applied on the lifetime of the B^0 meson, it is interesting to check if this value in Pythia corresponds with the accepted value. This can be done by plotting the distribution of lifetimes of the B^0 meson, called $c\tau$. For the signal, this distribution is described by a single exponential whose slope is the particles lifetime. This distribution is fitted in Figure 3.4 from which it can be concluded that the found value, 458.6 ± 1.6 µm/c corresponds with the accepted value 455.4 ± 2.0 µm/c. The same applies for the D^0 meson. So, the in this thesis applied cuts on the lifetime ($c\tau$) and distance to collision point (d_{PV}), are an identification for what can be used for the reconstruction in the ALICE experiment.

3.3 Transverse momentum smearing

Pythia gives insight in the vacuum particle production. All values are precisely known by the conversation laws. However, this is not the situation what will be measured in the ALICE experiment. Every detector has a resolution and so does the ALICE detector. An important resolution is the one in measuring the transverse momentum. To introduce this resolution effect in the simulations, the transverse momentum of all particles is smeared according to the improved ITS momentum resolution (showed in Figure 3.5).

To smear the p_T, a random Gaussian generator, provided by the Root Framework, is used. *TRandom3*, which is the name of this class, is a pseudorandom number generator

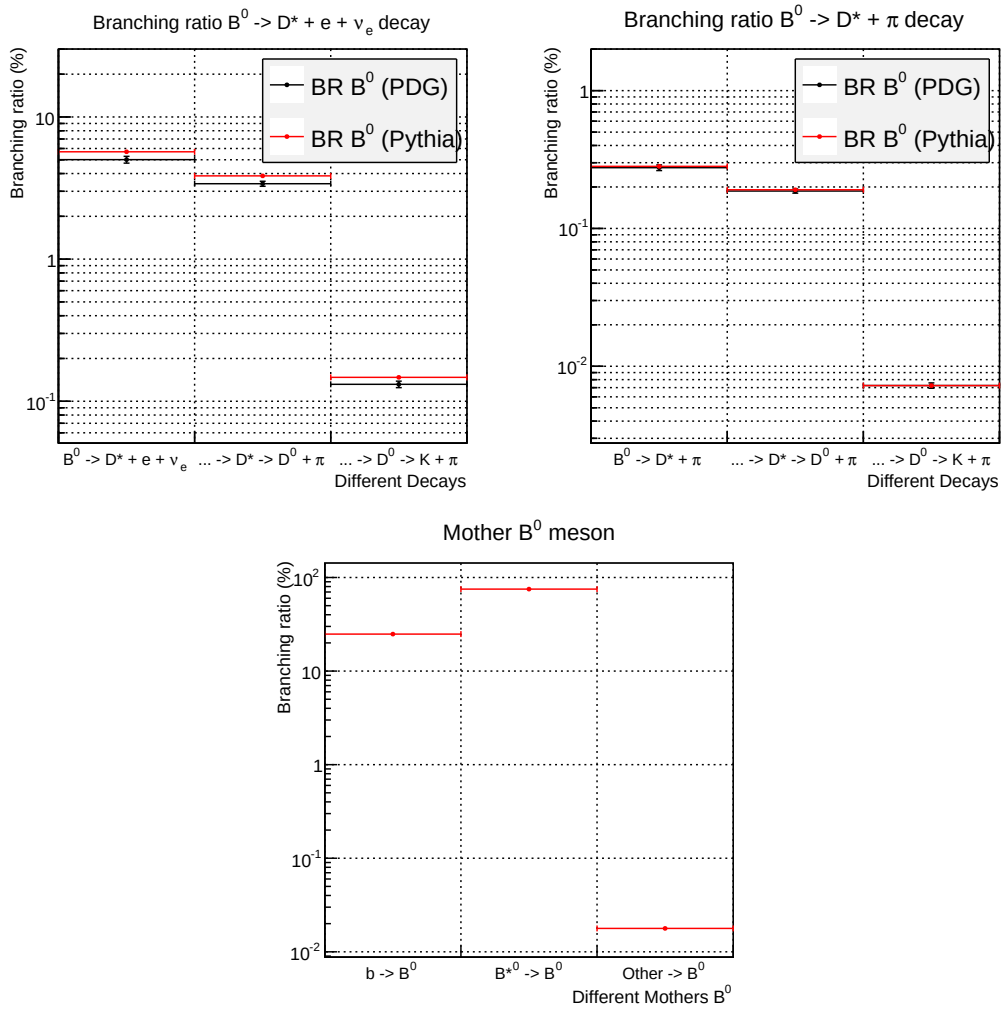

FIGURE 3.3: The mother particles for all the B^0 mesons (bottom plot) and a comparison between the calculated branching ratios in Pythia 8 and the accepted value from the Particle Data Group (upper plots) [25].

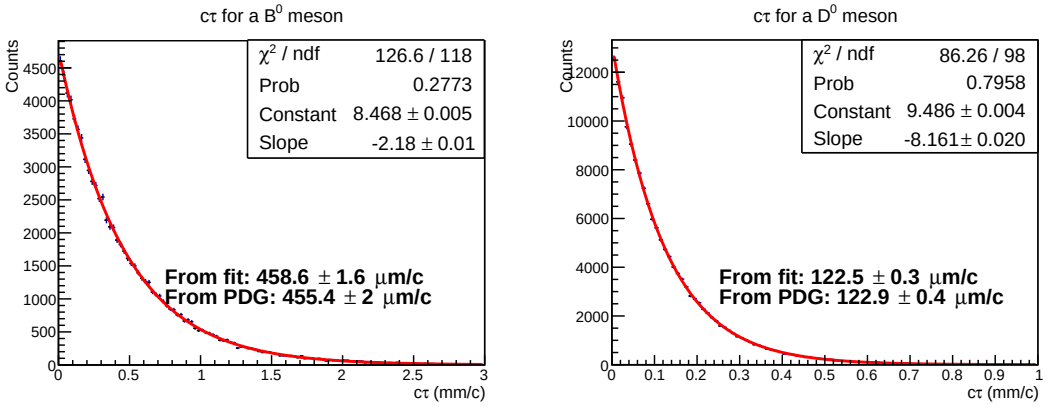

FIGURE 3.4: A fit to the $c\tau$ distribution of B^0 and D^0 mesons from which their lifetime (in μm/c) can be calculated.

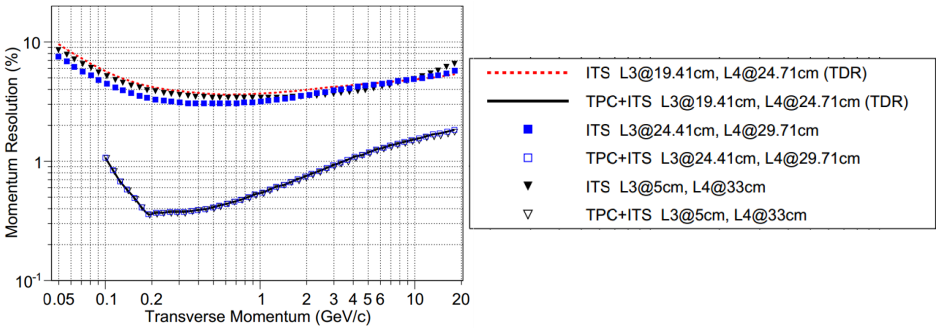

FIGURE 3.5: Performance of the ITS stand-alone and TPS+ITS combined reconstruction for different radial positions of the ITS layer. The upper blue line in the plot is used to smear the transverse momentum of the particles produced in the simulations [15].

(PRNG) class based on the Mersenne Twister method made by M. Matsumoto and T. Nishimura. It was designed specifically to correct most of the lacks found in older PRNGs. It is therefore working very well and provide fast generation of high-quality pseudorandom integers.

This smearing procedure will be fundamental to study the invariant mass distribution of the two decays as can be seen in Figure 3.6. Without the smearing the invariant mass distribution is a delta function at exactly the right mass. After smearing it becomes a Gaussian peak with a width of 110 MeV/c^2. This is approximately the same as what is expected to be measured in the ALICE detector.

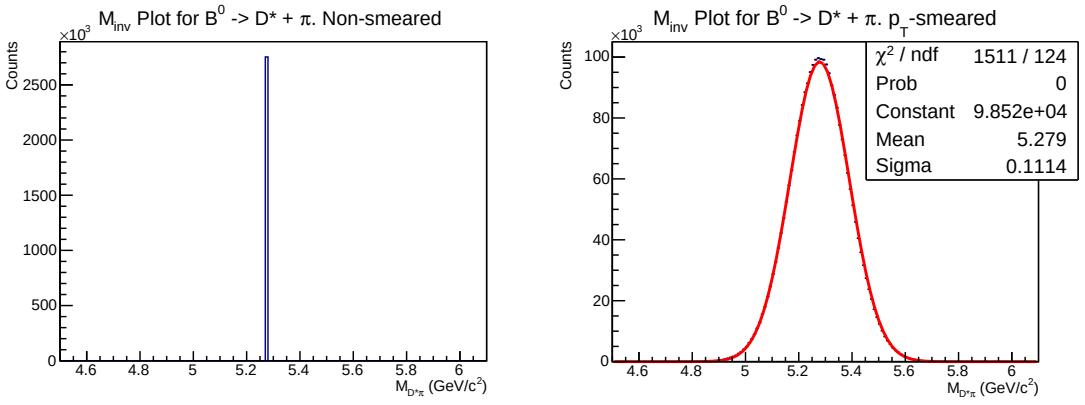

FIGURE 3.6: The effect of the smearing of the transverse momentum on the p_T integrated invariant mass distribution of the signal.

Chapter 4

Performance study of $B^0 \rightarrow D^{*+} + \pi^-$ decay

In this chapter, the results of the performance study with the event generator Pythia on one of the hadronic decay channels for a B^0 meson are presented. The behaviour of the beauty quarks at a 13 TeV proton-proton collision can be reconstructed by analysing the properties of the outcoming particles. The study into this decay is needed as preparation for when the data will be available in May 2015.

This chapter will start with a small study in the properties of the daughter particles from the B^0 meson. The reconstruction procedure and the applied selection cuts for this decay will be discussed after this. Before the results can be presented, a second smearing procedure needs to be added. This is the vertex distribution smearing according to the ITS pointing resolution. With these two types of smearing introduced, the results of the yield extraction through an invariant mass analysis for this decay will be presented. This chapter ends with a summary of the specific values for this decay in the different p_T intervals (for example the statistical significance of the signal).

4.1 Hadronic decay

The decay chain this chapter covers consists of three hadronic decays. The full chain is the following:

$$\begin{aligned} b\,(\rightarrow\, B^{*0}\,) \;\rightarrow\; B^0 \;&\rightarrow D^{*+} \;+\; \pi^- \\ &\hookrightarrow D^0 \;+\; \pi^- \;+\; \pi^+ \\ &\quad\hookrightarrow \pi^- \;+\; 2\pi^+ \;+\; K^-.\end{aligned}$$

The total branching ratio of this decay is quite low, $(3.04 \pm 0.4) \cdot 10^{-3}\%$, which is mainly due to the decay of the B^0 meson. This decay has a branching ratio of only $(0.276 \pm 0.013)\%$ [25]. Nevertheless, this decay chain is interesting to study heavy flavour production because there are only three particles to reconstruct. And in contrast to the decay studied in the next chapter, all final particles can be detected. So the laws

[1] The decays $B^0 \rightarrow D^{*-} + \pi^+$ and $D^0 \rightarrow K^+ + \pi^-$ are also included in this study.

of momentum and energy conservation will be sufficient for the reconstruction of the undetected D^0, D^{*+} and B^0 mesons.

To start the study into this decay, some properties of the three pions are investigated. This can be interesting because the distributions can have some particular behaviour that can be used as a cut parameter. The principle of cutting aims to decrease the combinatorial background of random pairs without having a large effect on the number of signal entries. The, for this decay used cut set, will be discussed in the next section.

For the three pions, the distribution of transverse momentum and the distance between production and collision point are investigated (showed in Figure 4.1). From these plots a few properties of the decay can be deduced. For example, the second pion (called π_{soft} or π_2 in the remainder of this thesis) is soft in comparison with the other two pions. This is because the π_{soft} is formed by an exited state of the D^+ meson, which decays into a D meson ground state. In such a decay, only a few hundreds MeV are left for the creation of the π_{soft}, which results in low p_T. So it is very unlikely to find a reconstructed decay chain where the second pion has $p_T > 3$ GeV/c, and therefore a selection cut can be placed on this parameter. In the reconstruction of a D^{*+} this cut is mostly performed by calculating the invariant mass of the π_{soft}, which will be discussed later.

Another interesting cut parameter that can be deduced from Figure 4.1 is the lifetime of the B^0 meson, or in other words the distance between the production point of the first pion (π_1) and the point where the collision point took place (called d_{PV} in the remainder of this thesis). This distribution peaks on a distance of 20 micrometers and decreases like an exponential function. The π_{soft} is formed at almost the same point as the π_1. This can be understood, given that the D^{*+} meson decays using the strong interaction and therefore has a very short lifetime ($c\tau = 0.1$ µm). The last pion (π_3) is produced further away from the collision point than the first two pions. So, in the reconstruction process $d_{PV}(\pi_3) > d_{PV}(\pi_1; \pi_2)$.

4.2 Performance study

Before the reconstruction of the collision can start, the identity of the measured particles is needed. The identification of a particle in the ALICE detector is performed, as described in Chapter 2, by the PID and TOF detector. All particles measured within 3σ of the expected value are included. With these final particles, a reconstruction of what happened after the collision can be made. In this thesis, this reconstruction is done by focussing on one particular decay and ignoring the other particles.

With only the kinematics and identity of the final particles it is impossible to determine which tracks corresponds to a real D^0, D^{*+} or B^0 decay. There is always a probability that three random pions and a kaon pair up to a potential B^0 meson. These events make up the combinatorial background. In real data, separating real B^0 mesons from combinatorial background is not possible, but in Monte-Carlo simulations this separation can be made. So Monte-Carlo simulations studies, like the one presented in this thesis, are useful in optimizing the reconstruction process and applied selection cuts.

In this thesis, a self-written code is used to create the combinatorial background, which is by approximation the same background as the one obtained by using the AliRoot framework. This combinatorial background is reconstructed by looking at the kinematics

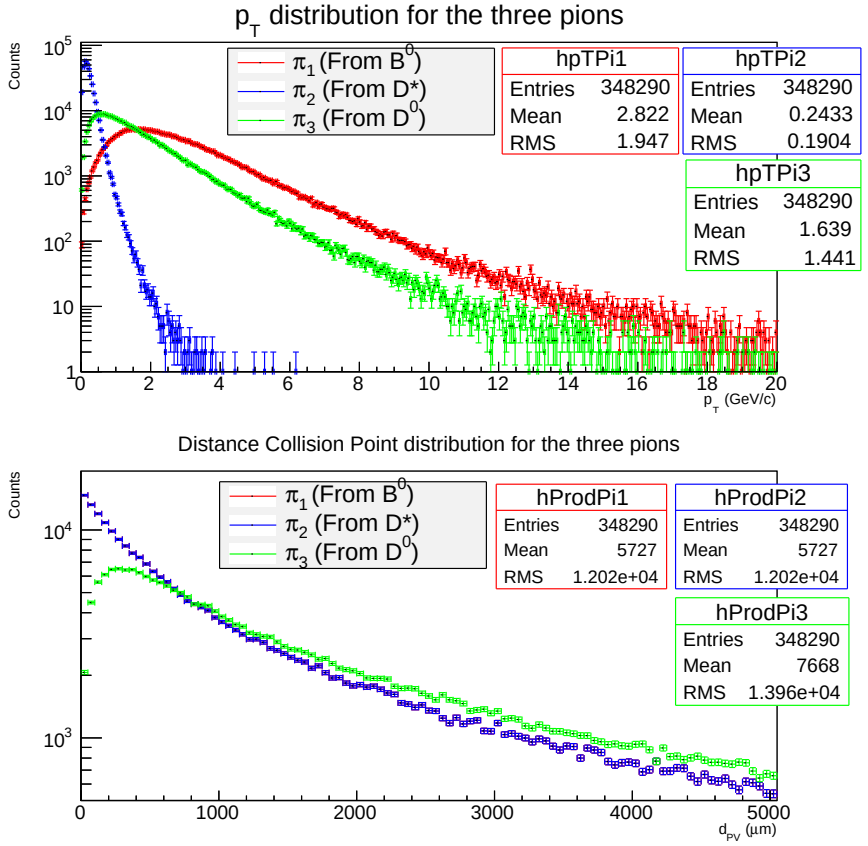

FIGURE 4.1: p_T and d_{PV} distribution for the three pions in the full decay chain of the B^0 meson.

and topology of the final pions and kaons. When the distance of closest approach (DCA) between a π^+ and K^- is smaller than 200 micrometers, which is approximately the resolution of the ALICE detector, it could be a pair with a D^0 meson as mother particle. A D^0 meson has $c\tau = 123$ µm, which results in a measurable displaced secondary vertex. The flightline of the D^0 meson between its vertices can be reconstructed from the momentum of the π^+ and K^-. Because the D^0 meson is neutral, its path is not affected by the Lorentz force and so the reconstructed momentum $\vec{p}_{\pi K}$ must point in the same direction as the flightline.[2] The flightline of the D^0 meson extends between 10 and 800 micrometers from its reconstructed point of decay halfway the DCA vector of the pion and kaon. When there is a second π^+, with DCA smaller than 200 micrometers with this flightline, a possible D^{*+} meson is reconstructed. Because the decay vertex of the D^{*+} meson can not be distinguished from its primary vertex, a π^-, again with DCA < 200 µm with the reconstructed point of production of the D^0 meson, pairs up to a potential B^0 meson. The momentum and energy of the reconstructed particles are calculated with the conservation laws of momentum and energy.

In a proton-proton collision at 13 TeV, there will be a large amount of final pions and kaons (in average 73.9 pions and 8.3 kaons when the events without pions or kaons are excluded). So, with the detectors resolution taken into account, the reconstruction will lead to a few possible B^0 mesons per event. This exceeds the number of real B^0 mesons per event with multiple factors, so ways to decrease the combinatorial background are

[2]There is no magnetic field in Pythia simulations, so all particles will have a straight path. However, in the ALICE detector, with its 0.5 Tesla magnet, only the neutral particles will have this property.

necessary. This is performed by placing selection cuts on the topological and kinematic information of the different particles. In the next subsection, the used cut set will be explained in more detail.

4.2.1 Topological cuts

Without proper selections, the B^0 signal would be comparable with statistical fluctuations of the combinatorial background and therefore be impossible to extract. The signal has to be greater than these fluctuations, which can be calculated with the statistical significance (S_g). This S_g is given by

$$S_g = \frac{S}{\sqrt{S+B}}, \tag{4.1}$$

where S and B are the number of entries of respectively signal and background in a regime around the position of the signal (mostly 2σ of 3σ). To maximise the statistical significance, an optimization of the cuts is needed. But because this thesis is only a first study into these B^0 meson decays a full optimization has not been done. The applied cuts are just an indication of what could be chosen as cut value, and therefore the statistical significance will be significantly higher after such an optimization.

Studies before in the measurement of charm production have resulted in a total of 16 topological cuts for the reconstruction of prompt D^{*+} [29–31]. They depend on the centrality of the collision and the transverse momentum of the D^{*+} meson . These selection cuts can, with a few adjustments, also be used for the second part of the decay chain studied in this thesis. For single tracks the important cuts are placed on the transverse momentum ($p_{T;\pi}$ and $p_{T;K}$) and the impact parameter ($d_{0;\pi}$ and $d_{0;K}$). For a pair of tracks, cuts can be applied on the distance of closest approach (DCA), the cosine of the decay angle ($\cos\theta_{decay}$), the cosine of the pointing angle ($\cos\theta_{pointing}$), the product of the impact parameters ($d_{0;\pi} \times d_{0;K}$) and on the invariant mass of mass difference $\Delta M = M_{D^{*+}} - M_{D^0}$). In this thesis, only a few selection cuts are used, which are specified in Table 4.1. Two of these cuts will now be further elaborated.

Name of cut	**Parameter [unit]**	**Abbr. Cut**
Pseudorapidity Coverage	$\lvert\eta\rvert < 0.9$	Eta
Z-coordinate cut	$\lvert z\rvert < 10$ [cm]	Z
Distance Closest Approach	DCA < 200 [µm]	Res
Lifetime D^0	$10 < c\tau < 800$ [µm]	dFly
Distance Collision Point π_1	$d_{PV;\pi_1} > 50$ [µm]	PV
Distance Collision Point π_2	$d_{PV;\pi_2} > 50$ [µm]	PV
Distance Collision Point π_3	$d_{PV;\pi_3} > 100$ [µm]	PV
Transverse momentum π_1	$p_{T;\pi_1} > 1.0$ [GeV/c]	pT
Mass difference D mesons	$142 < \Delta M < 149$ [MeV/c^2]	dM

TABLE 4.1: Selection cuts applied during the reconstruction of the B^0 meson. The abbreviations of the cuts will only be used in titles or legends in some figures.

A very effective cut is the one on the invariant mass difference of the D mesons. For a real D^{*+}, which decays into a D^0 and π^+, this peak will always be positioned at 145.5 MeV/c^2. So only slightly above the mass of the pion. However, for the combinatorial

background, this will be totally random. The ΔM distributions for the signal (left) and background (right) are shown in Figure 4.2. In this thesis, the cut is placed for ΔM lower than 142 MeV/c^2 and higher than 149 MeV/^{2}, which is indicated by the dashed lines. This leads to a decrease of 0.1 percent in signal and 99.6 percent in background.

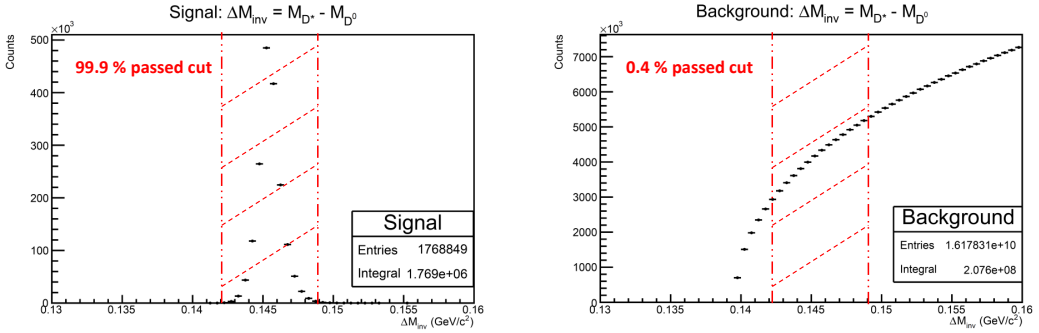

FIGURE 4.2: p_T integrated distribution of ΔM for signal (left) and background (right) with the selection cut indicated by the dashed lines and the percentage that passed the cut given in red.

Another effective cut is placed on the transverse momentum of the π_1, which have to be higher than 1 GeV/c. In Figure 4.1 the p_T distribution for the signal pions is already specified. This can be compared with the transverse momentum distribution of the combinatorial background as showed in Figure 4.3. The decrease in background (ΔB) and decrease in signal (ΔS) for the different p_T intervals are specified in the table next to this figure. The necessary selection cuts for the reconstruction process (the first four from Table 4.1) are used on the data for this Figure. The cut on $p_{T;\pi_1}$ is, obviously, more effective on the lower p_T intervals.

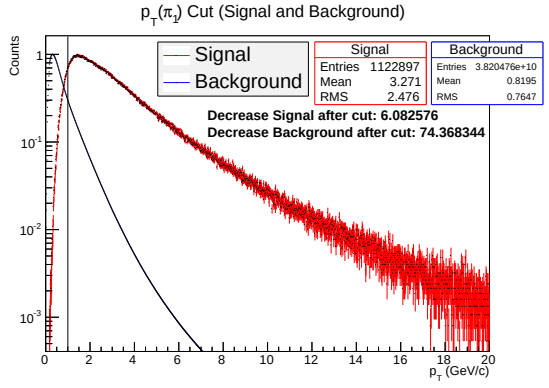

p_T interval (GeV/c)	ΔS (%)	ΔB (%)
0 - 3	0.12	78.56
3 - 6	6.22	54.11
6 - 10	9.14	48.27
10 - 15	5.26	48.99
15 - 20	3.33	49.35
20 - 30	2.27	52.27

FIGURE 4.3: Distribution of $p_{T;\pi_1}$ for the p_T integrated signal (red symbols) and background (blue symbols) and percentage decrease in entries for background and signal after applying the cut at 1 GeV/c (indicated by the black line). Because the cut is applied at low transverse momentum, both distributions are scaled to the same height. Therefore, the difference in maximum is clear.

The selection cuts on Distance Closest Approach and Distance Collision Point, are still a bit meaningless because the vertex distribution of the particles have not been smeared. This vertex smearing will be discussed in the next section. All the plots and results showed after this point are smeared in transverse momentum and vertex distribution. A brief summary of the results with only smearing of the transverse momentum can be found in Appendix A.

4.2.2 Vertex distribution smearing

The ALICE detector has a resolution in measuring the transverse momentum of particles, but it also has a resolution in track and vertex reconstruction. In Pythia, the exact points of formation and decay are known, but in real measurements this is not the case. So to give a realistic picture of the situation inside the ALICE detector, the vertex distribution in Pythia have to be smeared, too. This is done according to the upgraded ITS pointing resolution in the R_z and R_ϕ direction which is shown in Figure 4.4. The pointing resolution will decrease after track reconstruction. This means that the vertex of mother particles will be better known than the ITS pointing resolution would suggest.

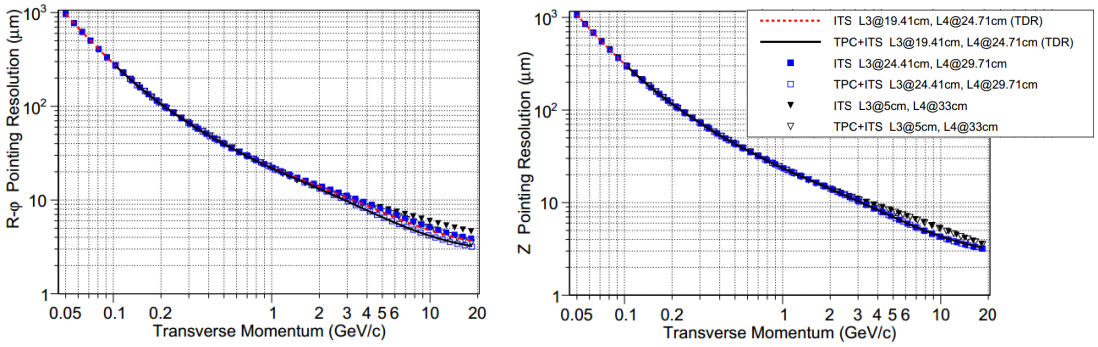

FIGURE 4.4: Performance of the ITS stand-alone and TPS+ITS combined reconstruction for different radial positions of the ITS layer [15].

Just like the smearing of the transverse momentum, the class *TRandom3* from the Root framework is used to smear the vertex distribution. In Figure 4.5, the difference between production point before and after smearing for three transverse momentum intervals is shown. They are all Gaussian distributed in both the R_z and R_ϕ direction, and the sigma of the peak decreases correctly according to the ITS pointing resolution.

With this type of smearing included, the cuts on DCA and Distance Collision Point make more sense. All the prompt pions can now pass the $d_{PV;\pi_1}$ cut what results in higher and more realistic combinatorial background. Another effect is that the probability of signal events with low p_T that do not pass the DCA cut becomes higher, which is of course also more realistic. The p_T integrated background increases with a factor 3.2 and the p_T integrated signal decreases with 18 percent after including the smearing of the vertex distribution.

4.2.3 Invariant mass distribution

The reconstruction and yield extraction of this decay is performed by using the invariant mass technique. The invariant mass of a particle is a Lorentz invariant characteristic of the total energy and momentum. It is calculated by

$$M_{inv} = \sqrt{(\sum_i E_i)^2 - |\sum_i \vec{p_i}|^2}, \tag{4.2}$$

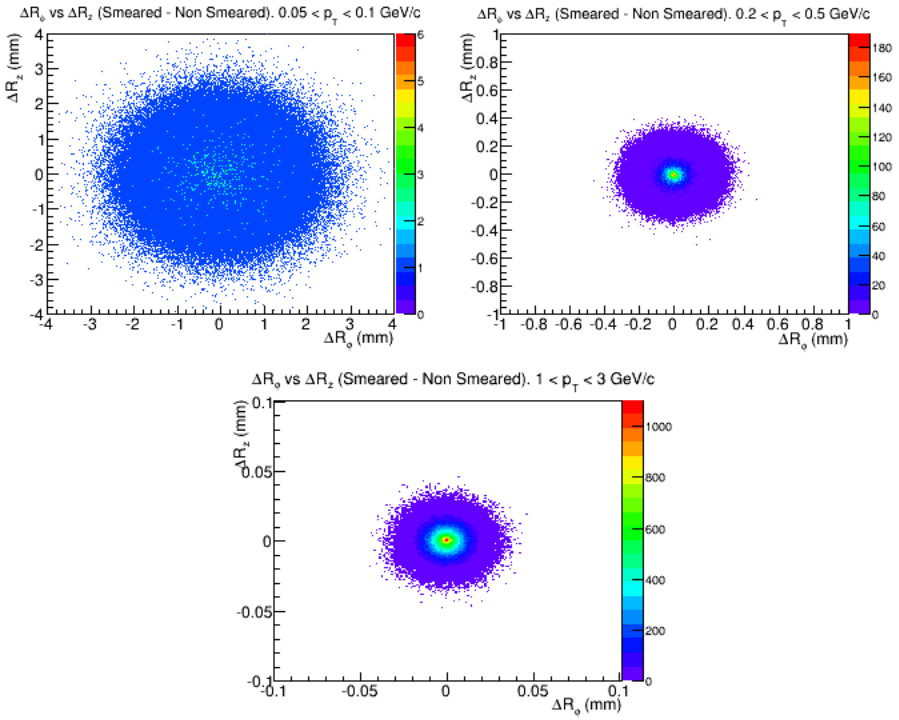

FIGURE 4.5: Difference in R_z and R_ϕ between production point before and after the smearing of the vertex distribution for three different p_T intervals (respectively 0.05 - 0.01, 0.2 - 0.5 and 1 - 3 GeV/c).

where i is a list with all the associated particles, $\vec{p}$ the particles momentum and E the energy of the particles calculated with $E = \sqrt{m_0^2 + \vec{p}^2}$. So, for example, the invariant mass of the D^0 meson is given by

$$M_{D^0} = M_{K\pi} = \sqrt{(E_K + E_\pi)^2 - |\vec{p_K} + \vec{p_\pi}|^2}. \tag{4.3}$$

In this thesis, the invariant mass distributions of signal and background are investigated in six different transverse momentum intervals. The signal invariant mass in transverse momentum interval 3 - 6 and 15 - 20 GeV/c are shown in Figure 4.6. The others look quite similar so are not shown in this thesis. The mean and sigma for the fitted Gaussian function for all the p_T intervals are shown on the right.

A fake reconstructed B^0 meson that passes the cuts will also give an entry in the invariant mass spectrum. However, this will be randomly distributed like an exponential function. The effect of the different selection cuts applied separately on the combinatorial background and signal are shown in Figure 4.7. The background decreases with 99.9993% but keeps having its exponential shape. The signal decreases only 17 percent after applying all selection cuts. The background invariant mass plots have a threshold at approximately 910 MeV/c^2 (which is three times the mass of the pion plus the mass of a kaon).[3]

[3]In Monte-Carlo simulations, it is an option to do not reconstruct the D^{*+}, but just ask for the real ones. In this case, the threshold for the invariant mass would be higher because the rest mass of the D^{*+} meson is already 2010 MeV/c^2.

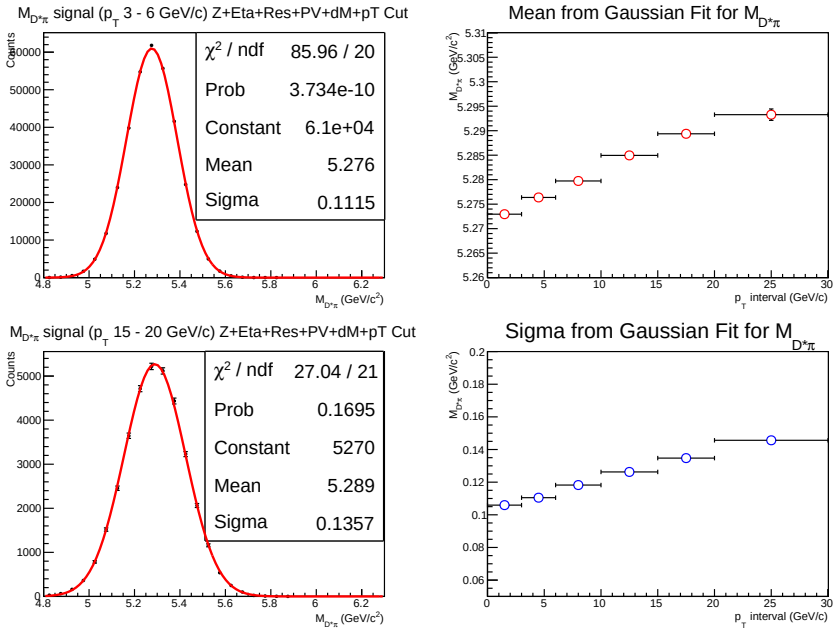

FIGURE 4.6: Left: Invariant mass plot for the investigated hadronic decay of a B^0 meson in two transverse momentum intervals (3 - 6 and 15 - 20 GeV/c). Right: Mean and sigma for the fitted Gaussian function for all p_T intervals.

When the two separate invariant mass distributions are added (after normalizing for the beauty forced configuration), the total number of events (in this thesis approximately 2.75 billion) is scaled up till the expected number of events for Run-2. These are 3.5, 35 and 350 billion proton-proton collisions. From the combined, normalized and scaled invariant mass spectra the yield of the decay can be obtained. This will be presented in the next section.

4.2.4 B^0 yield and statistical significance

To finalise the B^0 yield extraction, the signal and combinatorial background have to be separated in the invariant mass spectrum. This is done by fitting the combined invariant mass spectra. The fit function is a sum of a Gaussian function for the signal and an exponential decreasing function for the background. The fitting process is performed by the *Fitter* class provided by the Root framework. This class uses the following fit function for the signal:

$$f_{sig}(M) = a_1 e^{-\frac{(M-a_2)^2}{2a_3^2}}, \tag{4.4}$$

and for the background

$$f_{back}(M) = e^{a_1' + a_2' M}. \tag{4.5}$$

The variables a_i and a_i' are the free fitting parameters. The result of this fit for the p_T integrated invariant mass spectrum is shown in Figure 4.8. From this fit the yield and statistical significance can be calculated, which are given in the plot. Note that in this

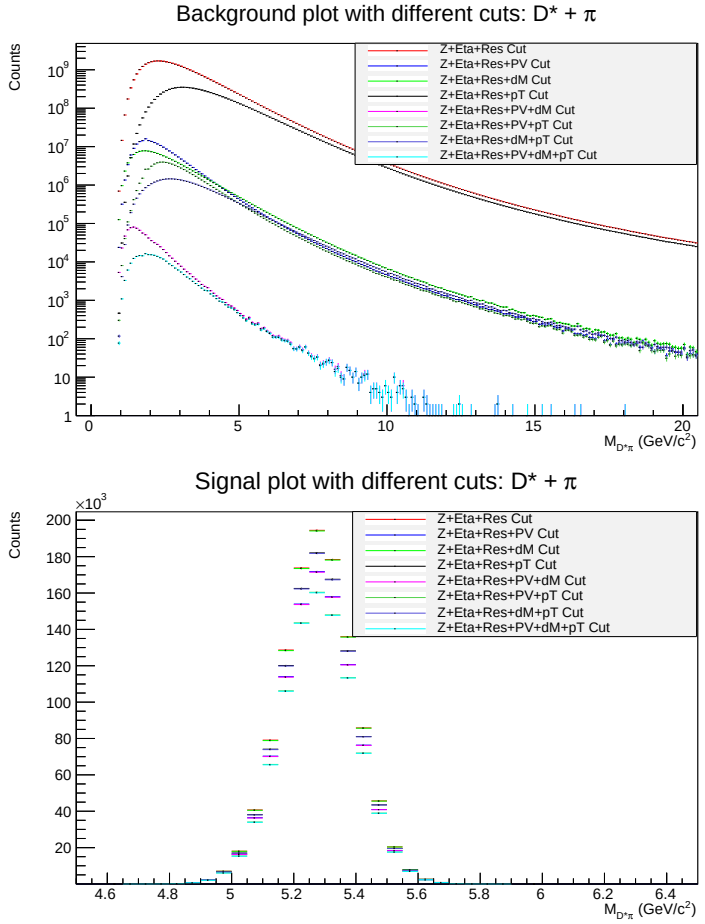

FIGURE 4.7: The effect of the different cuts on the p_T integrated combinatorial background (top) and signal (bottom) invariant mass plots for the investigated hadronic decay of the B^0 meson. The used abbreviations are specified in Table 4.1

plot the signal distribution is scaled up with a factor two. Otherwise the Gaussian peak was too low to fit. So this plot does not describe the real situation and can only be used as an indication for what can be expected when more selection cuts on the combinatorial background are applied.

Unfortunately, the combinatorial background in the separate transverse momentum intervals have limited statistics. Therefore, fitting the signal was not possible because of too large fluctuations in the background. So a different approach to calculate the statistical significance have been used. Instead of integrating beneath the fitted functions, the number of entries for signal and background were counted from the separate invariant mass spectra inside a 2 and 3σ interval. With these numbers the signal-over-background ratio S/B and statistical significance S_g can be calculated. These values are shown in Figure 4.9. To properly fit the signal, S_g have to be higher than 3. So, as can be seen in this figure, it will not be profitable to investigate this decay at 3.5 billion events. However, S_g increases proportional with $\sqrt{N} = \sqrt{N_{\text{new}}/N_{\text{old}}}$ (where N_{new} and N_{old} are the number of events). This means that at 35 billion events there will be a signal which can be fitted.

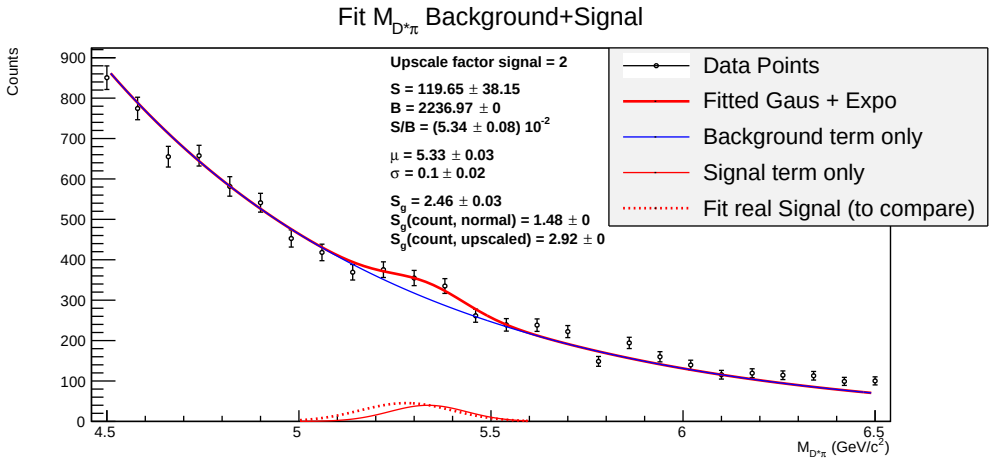

FIGURE 4.8: Signal fitted on the combinatorial background for the p_T integrated invariant mass spectrum. The signal is scaled up with a factor 2 because of too high combinatorial background. S_g(count) is calculated with the counting procedure and the dashed red line is the Gaussian function fit performed on the invariant mass distribution for the signal. Both are used to check the result obtained with the fit.

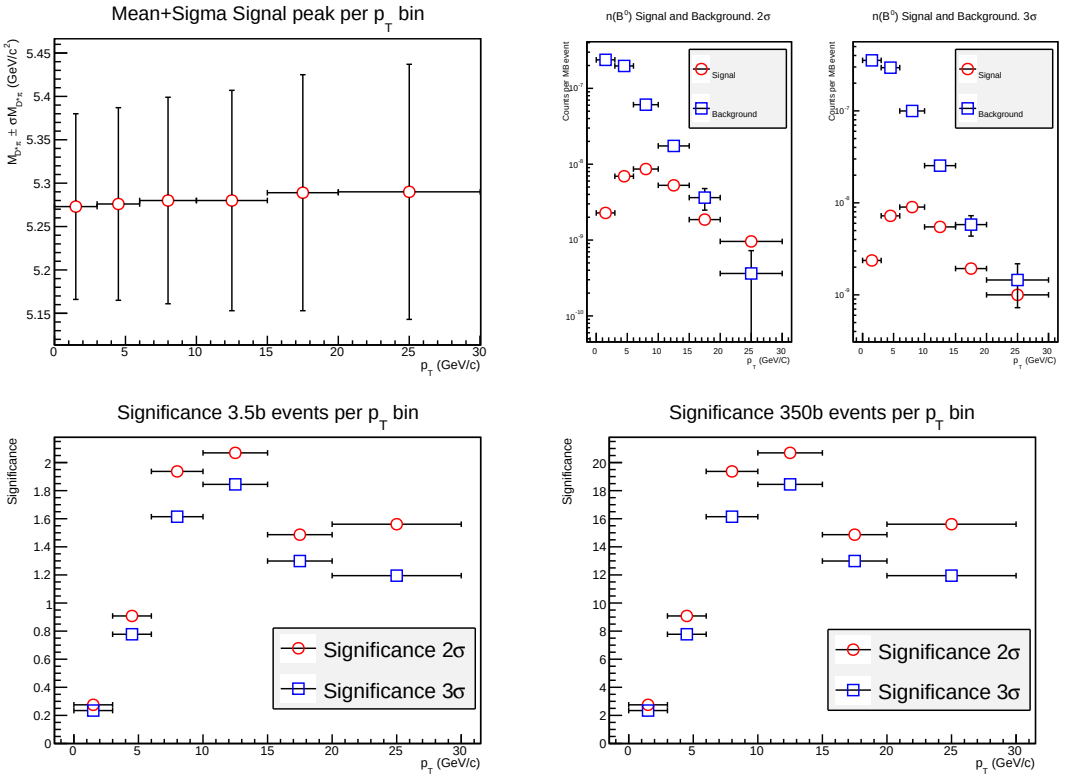

FIGURE 4.9: Mean and width of signal (upper left corner), counted number of S and B (upper right corner) and the statistical significance S_g for the six transverse momentum intervals for 3.5 (left) and 350 billion (right) proton-proton collisions at 13 TeV. Note that the error bars on the plot with the mean of the signal represent the sigma of the fit.

Chapter 5

Performance study of $B^0 \rightarrow D^{*+} + e^- + \bar{\nu_e}$ decay

In this chapter, the results of the performance study with event generator Pythia on one of the semi-leptonic decay channels for a B^0 meson are presented. A semi-leptonic decay of a meson refers to a decay channel where a lepton, its associated neutrino and a hadron (or multiple hadrons) are produced. Unfortunately, neutrinos can not be detected with the ALICE detector so a reconstruction method is needed to investigate a semi-leptonic decay. This chapter will start with an introduction in the studied decay, the used reconstruction method and its effect on the invariant mass distribution of the signal. This is followed by a short section about the used cut set, whereafter the results of the invariant mass analysis will be presented.

This semi-leptonic decay has not been investigated before to study heavy flavour production, so the results presented in this chapter will give an interesting first impression if it is profitable to study during Run-2. All the results presented in this chapter have been smeared in transverse momentum and vertex distribution except if stated otherwise. The final results with only smearing of the transverse momentum can be found in Appendix B.

5.1 Semi-leptonic decay

The decay chain this chapter covers consists of one semi-leptonic and two hadronic decays. The full chain is the following:

$$\begin{aligned} b\,(\rightarrow\ B^{*0}\,)\ \rightarrow\ B^0\ &\rightarrow D^{*+}\ +\ e^-\ +\ \bar{\nu_e} \\ &\hookrightarrow D^0\ +\ e^-\ +\bar{\nu_e}\ +\ \pi^+ \\ &\quad\hookrightarrow e^-\ +\bar{\nu_e}\ +\ 2\pi^+ +\ K^-.\end{aligned}$$

This decay is interesting to study because of the high branching ratio, which is approximately 18 times higher than the studied hadronic decay chain. The branching ratio, from beauty quark to final particles, is $(5.52 \pm 0.37) \cdot 10^{-2}\%$ [25]. This will lead, with the naive assumption that the reconstruction of the neutrino works perfect, to a higher S/B

[1] The decays $B^0 \rightarrow D^{*-} + e^+ + \nu_e$ and $D^0 \rightarrow K^+ + \pi^-$ are also included in this study.

ratio and statistical significance than for the $B^0 \to D^{*+} + \pi^-$ decay. So it is possible that this decay is already profitable to study beauty production at 3.5 billion events. But first the effect of the reconstruction of the neutrino has to be studied.

The used reconstruction method for the neutrino is inspired on a momentum reconstruction method used in the LHCb experiment [2]. The LHCb experiment studies multiple B meson decays, including semi-leptonic ones, to investigate CP violation. When they find a possible semi-leptonic decay of a B meson, this momentum reconstruction method is used to shift the invariant mass peak. Because, when the neutrino is ignored, a part of the momentum is discarded, which leads to an unobservable peak at low invariant masses where there is a high combinatorial background.

5.1.1 Reconstruction of the missing neutrino momentum

To reconstruct $\vec{p}_\nu$, the flightline of the B^0 meson (called $\vec{f}_{B^0}$) and the combined momentum $\vec{p}_{D^*e}$ have to be considered. For the same reason as $\vec{p}_{K\pi}$ has to point in the direction of the D^0 mesons flightline (as discussed in section 4.2), $\vec{p}_{B^0}$ must point in the $\hat{f}_{B^0}$ direction. Only, this time, this fact is used the other way around.

In a proton-proton collision no Quark-Gluon Plasma will be formed, so it can be assumed that the B^0 is formed at the collision point.[2] So the (assumed) point of formation, the (reconstructed) point of decay and a part of the B^0 meson momentum ($\vec{p}_{D^*e}$) are known. With this information the minimal required momentum for the neutrino, so that $\vec{p}_{B^0}$ points in the same direction as $\vec{f}_{B^0}$, can be calculated using geometry. This reconstruction method is illustrated in Figure 5.1 and summarized in the following set of equations (5.1 till 5.5). The production point for the B^0 meson is the collision point ($\vec{r}_{prod} = \{x_0, y_0, z_0\} = \{0, 0, 0\}$) and its point of decay is halfway the DCA vector of the D^{*+} meson and the e^- ($\vec{r}_{dec} = \{x, y, z\}$):

$$\theta_{B^0} = \arccos \frac{(z - z_0)}{|\vec{r}_{dec} - \vec{r}_{prod}|}, \tag{5.1}$$

$$\phi_{B^0} = \arctan \frac{(y - y_0)}{(x - x_0)}, \tag{5.2}$$

$$\vec{f}_{B^0} = \{\sin\theta_{B^0}\cos\phi_{B^0}, \sin\theta_{B^0}\sin\phi_{B^0}, \cos\phi_{B^0}\}, \tag{5.3}$$

$$\vec{p}_{\parallel;D^*e} = \mathrm{proj}_{\vec{f}_{B^0}}(\vec{p}_{D^*e}) = \frac{(\vec{p}_{D^*e} \cdot \vec{f}_{B^0})}{|\vec{f}_{B^0}|^2}\vec{f}_{B^0}, \tag{5.4}$$

$$\vec{p}_\nu = \vec{p}_{\parallel;D^{*+}e^-} - \vec{p}_{D^{*+}e^-}. \tag{5.5}$$

To study the pure effect of this reconstruction method, the non-smeared data have to be considered. This is because the two smearing procedures introduce some extra errors in the calculation of $\vec{f}_{B^0}$ and $\vec{p}_\nu$. In Figure 5.2, the invariant mass plot for three situations in transverse momentum interval 0 - 3 GeV/c are shown. These three plots make the necessity of adding a reconstructed $\vec{p}_\nu$ clear. When the neutrino is simply ignored the invariant mass distribution changes from a delta peak at the correct B^0 meson mass to

[2] This assumption will still be correct for the decay $b \to B^{*0} \to B^0$ because the very short lifetime of the B^{*0} meson

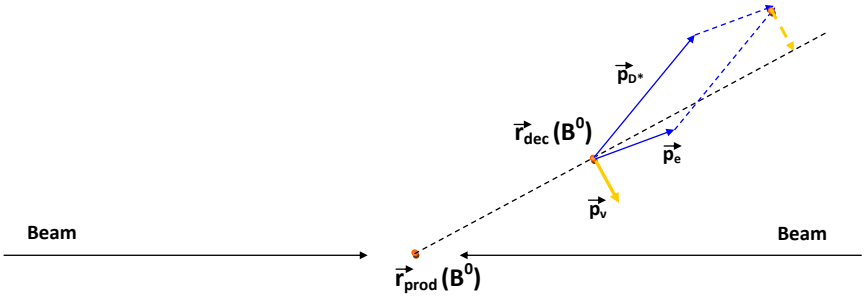

FIGURE 5.1: Schematic description of the reconstruction of $\vec{p}_\nu$.

a randomly distributed spectrum between the two thresholds ($M_{D^{*+}} + M_{e^-}$ and M_{B^0}). This peak is very wide and is positioned at a position where it can not be excluded from the background. After adding the reconstructed $\vec{p}_\nu$ the invariant mass peak shifts towards higher invariant masses.

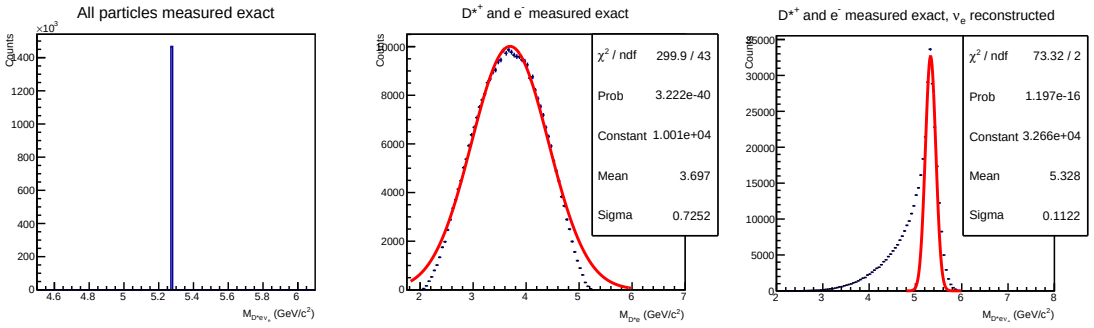

FIGURE 5.2: Effect of reconstructing $\vec{p}_\nu$ for p_T interval 0 - 3 GeV/c (note the different ranges on the x axis). Left: Unrealistic situation where all $\vec{p}$ are measured exact. Middle: $\vec{p}_{D^{*+}}$ and $\vec{p}_{e^-}$ measured exact and $\vec{p}_\nu$ ignored. Right: $\vec{p}_{D^{*+}}$ and $\vec{p}_{e^-}$ measured exact and $\vec{p}_\nu$ reconstructed.

For the 0 - 3 GeV/c p_T interval, the reconstructed peak becomes centered around the mass of the B^0 meson and the width of the peak decreases with a factor 6. For higher p_T intervals, the peak becomes wider and centered around higher values. The part that make up this increasing width in the non-smeared invariant mass plots is the missing momentum in the $\hat{f}_{B^0}$ direction. The neutrino adds zero to the momentum in this direction, but that is, obviously, not true for most events. The probability if the reconstructed $\vec{p}_{B^0}$ is too large or small depends on the angle between the momentum of the real neutrino and $\vec{f}_{B^0}$. For angles smaller than 90°, which are more likely to occur (see upper plots Figure 5.3), the reconstructed $\vec{p}_{B^0}$ is too small in comparison with the real momentum and vice versa for angles bigger than 90°.

The total energy of the reconstructed $\bar{\nu}_e$ can never be higher than the energy of the original neutrino, because $\vec{p_\nu}$ in the $\hat{f}_{B^0}$ direction is always zero. This too low E_ν will have a larger effect on E_{B^0} for low $p_{T;B^0}$ than for higher transverse momentum. This is because of the simple reason that E_{D^*} and E_e increase faster for higher p_T than E_ν because these particles have a higher mass. So the difference in E_ν will have less impact on E_{B^0}. This means for the invariant mass calculation that, $|\vec{p}_{B^0}|^2$, which is more often too small because of the $\vec{p}_\nu$-$\hat{f}_{B^0}$ angle distribution, is subtracted from $E^2_{B^0}$, which will always be too small. These two variables are related ($\Delta(E^2_{B^0}) - \Delta|\vec{p}|^2$ switches for particular p_T from sign), which causes a tail for the low p_T intervals and a shift towards

$\mathbf{p_T}$ **interval (GeV/c)**	**ΔS (%) ($\mathbf{d_{PV}}$)**	**ΔB (%) ($\mathbf{d_{PV}}$)**	**ΔS (%) ($\mathbf{p_T}$)**	**ΔB (%) ($\mathbf{p_T}$)**
0 - 3	22.5	99.2	12.9	81.9
3 - 6	8.2	99.5	10.5	69.9
6 - 10	5.0	99.1	6.6	65.0
10 - 15	3.4	98.8	3.7	64.7
15 - 20	2.2	98.9	2.4	64.8
20 - 30	1.8	99.1	1.5	62.8

TABLE 5.1: Percentage decrease in entries for signal and background after applying a cut on $d_{PV;e^-}$ or $p_{T;e^-}$.

high invariant masses for the high p_T intervals. This switch in sign is shown in the bottom plots in Figure 5.3. For low p_T, E_{B^0} overcompensates the lower momentum, so there are too many events with M_{B^0} too low and therefore a tail at the left end of the invariant mass distribution appears. For high p_T intervals the difference in the $|\vec{p}_{B^0}|^2$ part will prevail, which leads to a widening and a shift of the peak towards higher invariant masses (see Figure 5.5).

So this reconstruction method is necessary for this semi-leptonic decay to study beauty production because otherwise the peak is positioned at too low M_{B^0}. However, the reconstruction method is not ideal because of this tail at low p_T and the shift towards higher invariant masses for high p_T intervals. This will make it harder to fit the signal on the combinatorial background.

5.2 Performance study

5.2.1 Topological cuts

The reconstruction of the D^{*+} is the same as described in Chapter 4 and the used cut set is the same as specified in Table 4.1. Only for this decay the transverse momentum cut $p_{T;\pi_1} > 1.0$ GeV/c is changed into $p_{T;e} > 0.6$ GeV/c. The $p_{T;e}$ distribution look quite the same as the $p_{T;\pi_1}$ distribution plot for signal and background in Figure 4.3, so only the percentage of decrease in entries per p_T interval are given (see right column Table 5.1).

The cut on the Distance Collision Point for e^- ($d_{PV;e^-} > 50$ µm) will now be explained further. In Figure 5.4, the p_T integrated $d_{PV;e}$ distribution for signal and background are plotted on top of each other. A bump in the background distribution can be seen at low d_{PV}. This bump is due to the (smeared) prompt electrons. Fortunately, 99.2% of the background, which include almost all these prompt electrons, are dropped by this selection cut. The percentage of decrease in entries per p_T interval for signal and background are specified in the middle column in Table 5.1. There is a possibility to make this cut tighter for the higher p_T intervals, because $c\tau(B^0) = 455 \pm 2$ µm.

5.2.2 Invariant mass distribution

Due to the two smearing procedures, $\vec{p}_{B^0}$ will not point precisely in the $\hat{f}_{B^0}$ direction. This leads to small errors in the calculation of the invariant mass, which will broaden the signal. This wider peak will decrease the negative effect of the reconstruction method

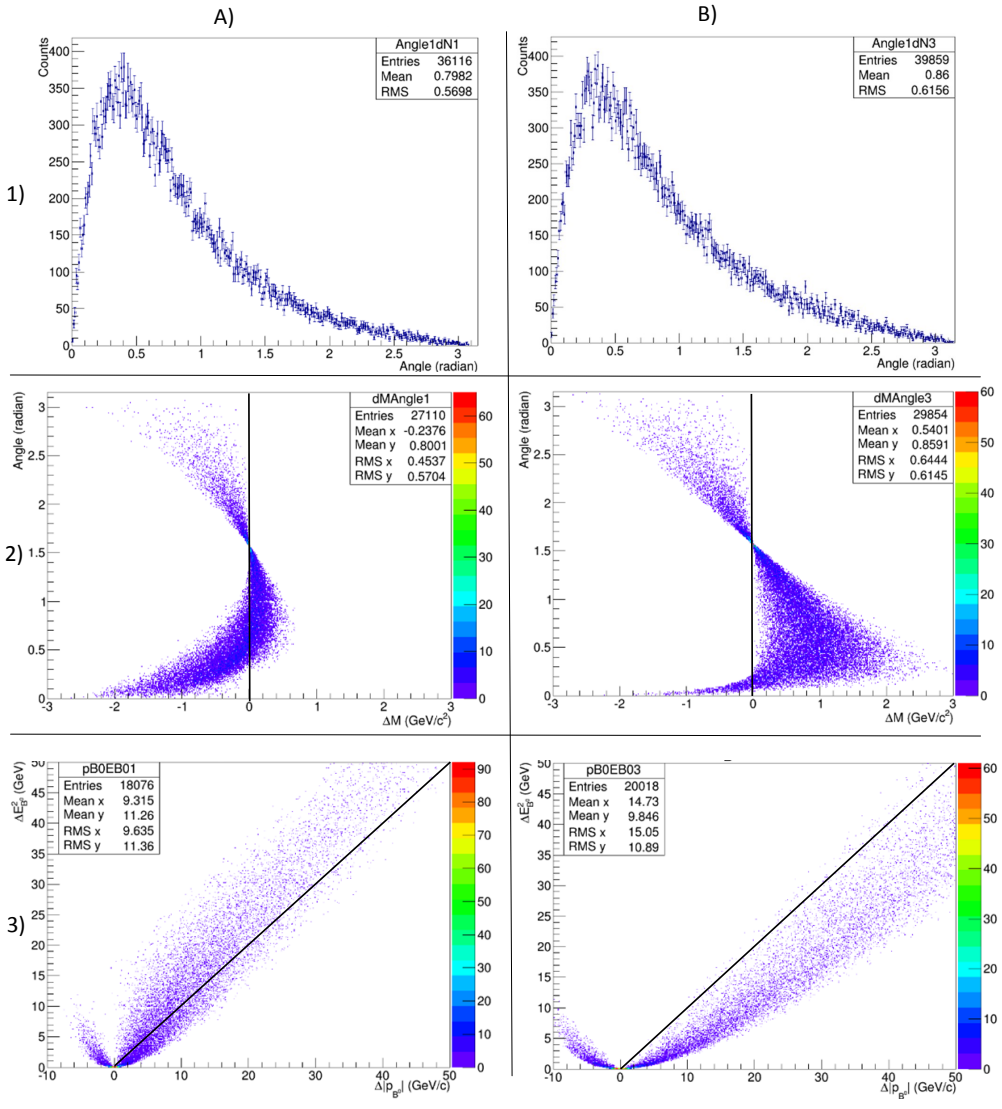

FIGURE 5.3: Explanation for the tail and shift in the invariant mass spectrum after reconstructing $\vec{p}_{\nu_e}$. Column a) is for the p_T interval 0 - 3 GeV/c and column b) for 6 - 10 GeV/c. Row 1) indicates the angle distribution between $\vec{p}_{\nu;\text{real}}$ and $\vec{f}_{B^0}$. The second row gives the dependency between $M_{B^0} - m_{B^0}$ versus this angle. The black line indicates the place where the correct mass is found. Row 3) describes the relation between $(E_{B^0;\text{real}})^2 - (E_{B^0})^2$ and $|\vec{p}_{B^0;\text{real}}|^2 - |\vec{p}_{B^0}|^2$. Again the black line indicates the events where the correct mass is found. The change from above (so $\Delta(E)^2 > \Delta|\vec{p}|^2$, which causes a tail) to beneath this line (so $\Delta(E)^2 < \Delta|\vec{p}|^2$, which causes the shift) can clearly be seen in these plots.

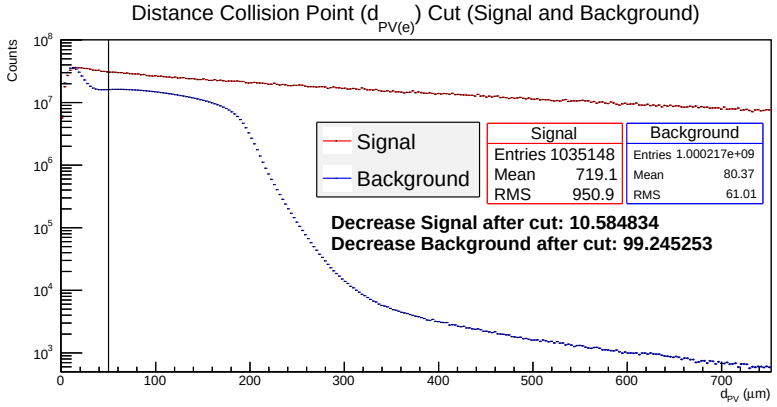

FIGURE 5.4: p_T integrated distribution of $d_{PV;e}$ for signal and background. To make the differences between the two distributions clear, the signal distribution is scaled up to the same height as the background distribution.

on the lower p_T intervals, the tail. But for the higher transverse momentum intervals, where the peak was already wide, this broadening will lead to a signal with $\sigma > 1.0$ GeV/c^2. So it will be hard to see anything at all on the combinatorial background. In Figure 5.5, the fitted (with the tail excluded) invariant mass distributions for the signal are shown for transverse momentum interval 3 - 6 and 15 - 20 GeV/c. On the right side, the mean and sigma of all the fitted Gaussian peaks are shown. The shift towards higher invariant masses and the increasing width for the higher transverse momentum intervals can be clearly seen.

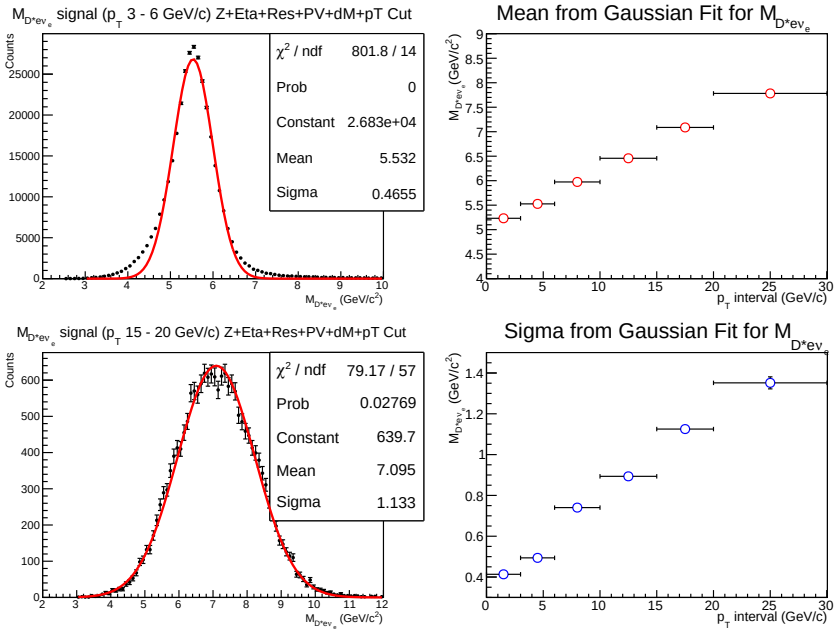

FIGURE 5.5: Left: Invariant mass plot for the investigated semi-leptonic decay of a B^0 meson in two transverse momentum intervals (3 - 6 and 15 - 20 GeV/c). Right: Mean and Sigma for the fitted Gaussian function for all p_T intervals. The fits have been performed by excluding the tail.

The p_T integrated invariant mass plots, with the different selection cuts applied separately, for the background and signal are shown in Figure 5.6. The background decreases

99.9986% and the signal decreases only 17.7% after applying all cuts.

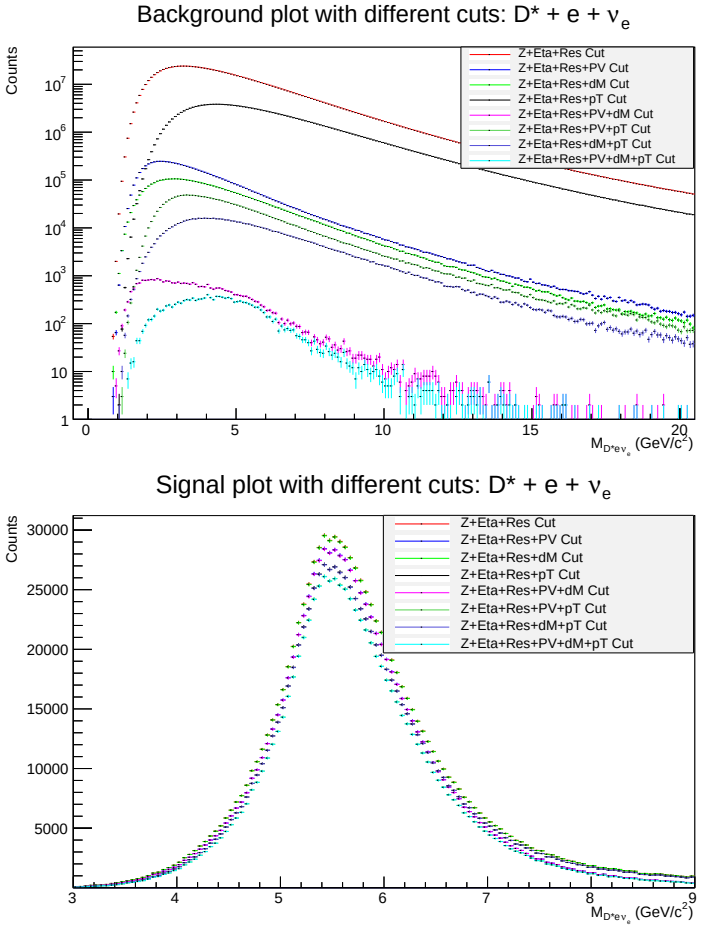

FIGURE 5.6: The effect of the different cuts on the p_T integrated combinatorial background (top) and signal (bottom) invariant mass plots for the investigated semi-leptonic decay of the B^0 meson. The used abbreviations are specified in Table 4.1

5.2.3 B^0 yield and statistical significance

To finalise the B^0 yield extraction, the signal and combinatorial background have to be separated in the invariant mass spectrum. So just as for the hadronic decay a Gaussian function have been fitted on the background (both scaled to the expected 3.5, 35 and 350 billion events). The background is described by a combination of an exponential, Landau and Gaussian function. In Figure 5.7, the fit on the p_T integrated combined invariant mass spectrum scaled up to 3.5 billion is shown.

Unfortunately, because of limited statistics and therefore too large fluctuations in the combinatorial background, this fitting procedure did not work for the six transverse momentum intervals. Besides this, there was another issue with the peak of the combinatorial background distribution. This peak is positioned close to the signal, which make it hard to see where the Gaussian peak is placed. This issue (at its worst) is illustrated in Figure 5.8 where the p_T interval 6 - 10 GeV/c is fitted by looking at the separate invariant mass distributions.

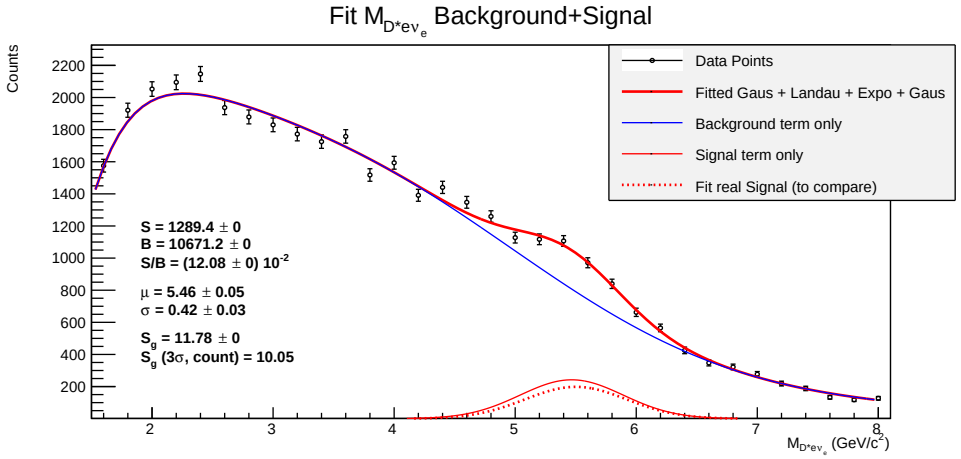

FIGURE 5.7: Fit performed on the combined, p_T integrated invariant mass spectrum of the signal and combinatorial background. S_g(count) is calculated with the counting procedure and the dashed red line is the Gaussian function fit performed on the invariant mass distribution for the signal. Both are used to check the result obtained with the fit.

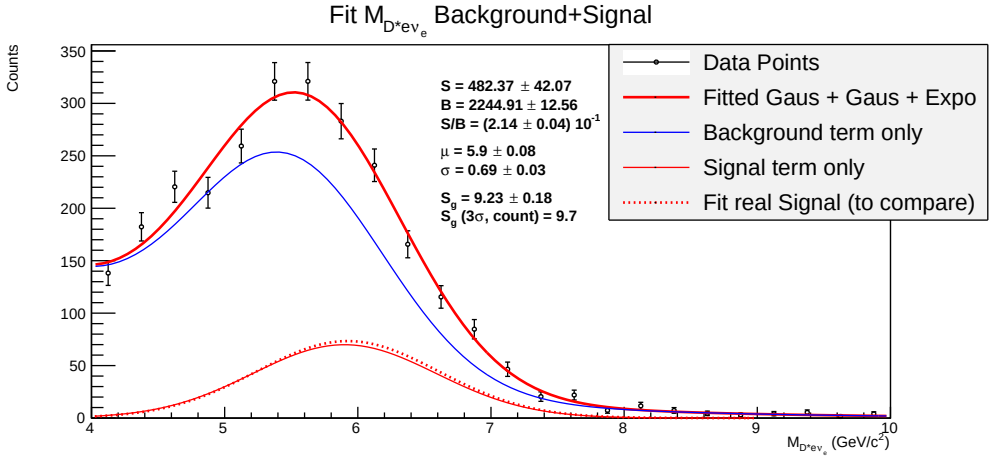

FIGURE 5.8: Fit performed on the invariant mass spectrum of the signal and combinatorial background in p_T interval 6 - 10 GeV/c. The background peaks at approximate the same position as the signal, which make is extremely hard to perform the invariant mass technique. Note that this is just an example plot where the fit only succeeded (indicated by the dashed red line) because there was access to the separate invariant mass spectra.

Because it is hard to fit the different invariant mass spectra for the p_T intervals, the counting procedure is used to calculate the statistical significance. The results are shown in Figure 5.9. Note that 2 and 3σ correspond now to a larger interval because the peak is wider than for the hadronic decay chain. As can be seen, the statistical significance for the different p_T intervals are already at 3.5 billion collisions higher than 3. This indicates that the signal can, when a solution for the few issues is found, be easily extracted over the background fluctuations.

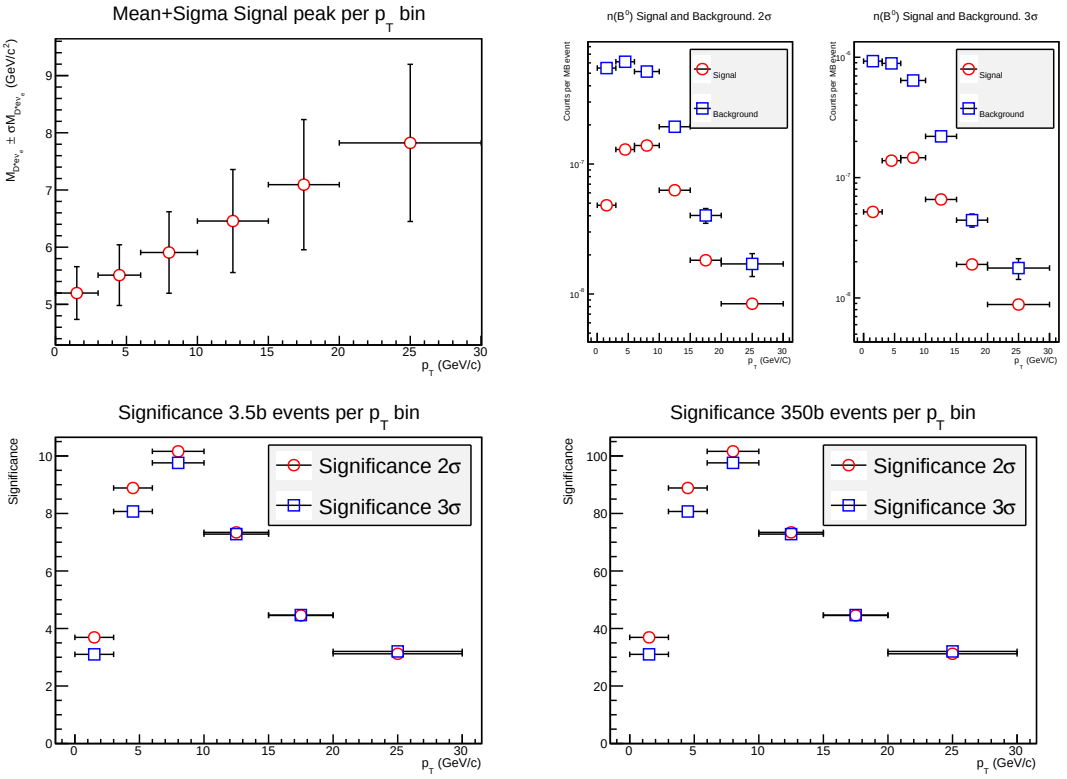

FIGURE 5.9: Mean and width of the signal (upper left corner), counted number of S and B (upper right corner) and the statistical significance S_g for the six transverse momentum intervals for 3.5 (left) and 350 billion (right) proton-proton collisions at 13 TeV. Note that the error bars on the plot with the mean for the signal represent the sigma of the fit.

Chapter 6

Conclusions and outlook

In this thesis, a performance study of two decays of the B^0 meson in proton-proton collisions at $\sqrt{s} = 13$ TeV have been done using the invariant mass analysis technique. The data for this analysis is obtained with the Monte-Carlo event generator Pythia, tuned to reproduce data, which the ALICE detector at CERN will start to obtain in May 2015. The simulations performed in this thesis are in good agreement with calculations performed with the FONLL computation framework. The produced beauty quarks are a bit softer, but that does not effect the results of this thesis. Properties of the B^0 meson like the branching ratio or decay length ($c\tau$) are not significantly different from the accepted value from the Particle Data Group. Only the branching ratio for $B^0 \rightarrow D^{*+} + e^- + \bar{\nu}_e$ is approximately 14 percent to high. This percentage have not been taken into account in Table 6.2.

For the studied semi-leptonic decay channel a reconstruction procedure for the undetected neutrino is needed. The reconstruction method is based on a recent technique used by the LHCb experiment. The position of the signal is shifted, due to this reconstruction, from low (approximately between the two thresholds $M_{D^{*+}} + M_{e^-}$ and M_{B^0}) towards higher invariant masses. At this new position, the combinatorial background is substantially lower. For low and high $p_T(B^0)$ will arise some issues with this reconstruction procedure, because of a particular angle distribution between the momentum of the real neutrino and the flightline of the B^0 meson. For the low p_T intervals, there arises a tail at the left end of the invariant mass distribution. For the higher p_T intervals, the width of the signal increases, which is associated with a shift of the peak position. Both these issues make it difficult to fit the invariant mass spectrum, but because of the high branching ratio of this decay fitting is, in principle, still possible.

The results of the invariant mass analysis technique are summarized in Table 6.1 and 6.2 for the six different transverse momentum intervals. These values are calculated by counting the number of events within 3σ of the peak position for the separate invariant mass distributions. This is done after scaling up the event statistics to the expected 3.5 billion collisions (the simulation data consisted out of 2.75 billion proton-proton collisions). The number of decays inside the pseudorapidity range of the ALICE detector ($|\eta| < 0.9$) are specified in the second column, and the number of decays that passed the selection cuts (specified in Table 4.1) in the third column. The statistical significance for the three different number of events and the signal-to-background ratio are also calculated with this set of selection cuts.

p_T **interval (GeV/c)**	**S(η range)**	**S(cut)**	**S/B**	S_g**(3.5b)**	S_g**(35b)**	S_g**(350b)**
0 - 3	$1.1 \cdot 10^1$	8.2	$6.6 \cdot 10^{-3}$	0.2	0.6	2
3 - 6	$3.1 \cdot 10^1$	$2.5 \cdot 10^1$	$2.5 \cdot 10^{-2}$	0.8	2.5	8
6 - 10	$3.8 \cdot 10^1$	$3.1 \cdot 10^1$	$9.0 \cdot 10^{-2}$	1.6	5.1	16
10 - 15	$2.1 \cdot 10^1$	$1.9 \cdot 10^1$	$2.2 \cdot 10^{-1}$	1.8	5.7	18
15 - 20	7.3	6.8	$3.3 \cdot 10^{-1}$	1.3	4.1	13
20 - 30	3.7	3.5	$6.8 \cdot 10^{-1}$	1.2	3.8	12

TABLE 6.1: Results of the invariant mass analysis of the decay $B^0 \rightarrow D^{*+} + \pi^- \rightarrow D^0 + \pi^- + \pi^+ \rightarrow \pi^- + 2\pi^+ + K^-$.

p_T **interval (GeV/c)**	**S (η range)**	**S (cut)**	**S/B**	S_g**(3.5b)**	S_g**(35b)**	S_g**(350b)**
0 - 3	$2.4 \cdot 10^2$	$1.8 \cdot 10^2$	$5.6 \cdot 10^{-2}$	3.1	9.8	31
3 - 6	$5.6 \cdot 10^2$	$4.9 \cdot 10^2$	$1.5 \cdot 10^{-1}$	8	25.3	80
6 - 10	$5.6 \cdot 10^2$	$5.1 \cdot 10^2$	$2.3 \cdot 10^{-1}$	9.8	31	98
10 - 15	$2.4 \cdot 10^2$	$2.3 \cdot 10^2$	$3.3 \cdot 10^{-1}$	7.5	23.7	75
15 - 20	$6.9 \cdot 10^1$	$6.7 \cdot 10^1$	$3.6 \cdot 10^{-1}$	4.2	13.3	42
20 - 30	$3.2 \cdot 10^1$	$3.1 \cdot 10^1$	$4.2 \cdot 10^{-1}$	3.0	9.5	30

TABLE 6.2: Results of the invariant mass analysis of the decay $B^0 \rightarrow D^{*+} + e^- + \bar{\nu_e} \rightarrow D^0 + \pi^+ + e^- + \bar{\nu_e} \rightarrow K^- + 2\pi^+ + e^- + \bar{\nu_e}$.

The number of the B^0 hadronic decays that will fall inside the range of the ALICE detector for 3.5 billion events is very low (less than 30 in all p_T intervals). This leads to low statistical significance, and it will therefore not be profitable to investigate this decay. However, for the number of events that are expected after 2015 (35 billion), this decay becomes interesting. The easy reconstruction and the exponential shape of the combinatorial background results in a signal that can be fitted. The used cuts are not yet optimized, so an even higher S_g can be expected. However, because the small number of decays inside the η-range, the used selection cuts can not become too tight.

The higher branching ratio for the semi-leptonic decay channel of the B^0 meson leads to high S and S_g. Already at 3.5 billion events this decay is interesting to study beauty production. Only the broad and shifted signal, as discussed above, is an issue. But as shown in this thesis, it is possible to fit it on the combinatorial background. This fit will become better with more events, because the statistical fluctuations of the background will become smaller. Also for this decay will an optimization of the selection cuts result in even higher S_g.

This thesis is concluded with a brief outlook, because research never truly finish. The performance study into these two decays was just a pilot study where the resolution and efficiencies of the ALICE detector were introduced by the smearing procedures. The results of this study look promising, but to refine them a full AliRoot simulation is needed. Also, the applied selection cuts need to be optimized and new ones need to be added. For example, the cut on the impact parameter for the B^0 meson. Because there is no magnetic field in Pythia simulations, this cut was no option for this thesis, but it can be very effective to decrease the combinatorial background further.

Another issue that should be studied are other decays from B mesons that are partially the same as the two investigated in this thesis. For example $B^+ \rightarrow D^{*+} + \pi^+ + e^- + \bar{\nu_e}$, which has a branching ratio of $(0.61 \pm 0.06)\%$. This incomplete decay will cause a small bump on the combinatorial background just before the region where the signal is positioned. This bump will make it harder to fit the combined invariant mass spectrum. A study to exclude this bump is important.

Appendix A

Results for the decay $B^0 \to D^{*+} + \pi^-$ with p_T smearing only

The final results for the invariant mass analysis technique, for the hadronic decay of the B^0 meson with p_T smearing only, are summarized in this chapter. This can be used as a comparison with the results described in Chapter 4. The fitted invariant mass distributions for the signal can be found in Figure A.1. The effect of the used selection cuts on the p_T integrated invariant mass distribution for signal and background is specified in Figure A.2. Unfortunately, as can be seen in this plot, the fluctuations in the combinatorial background were too large. Therefore, the final results for the different p_T intervals (see Figure A.3) are calculated using the counting procedure as explained in Chapter 4.

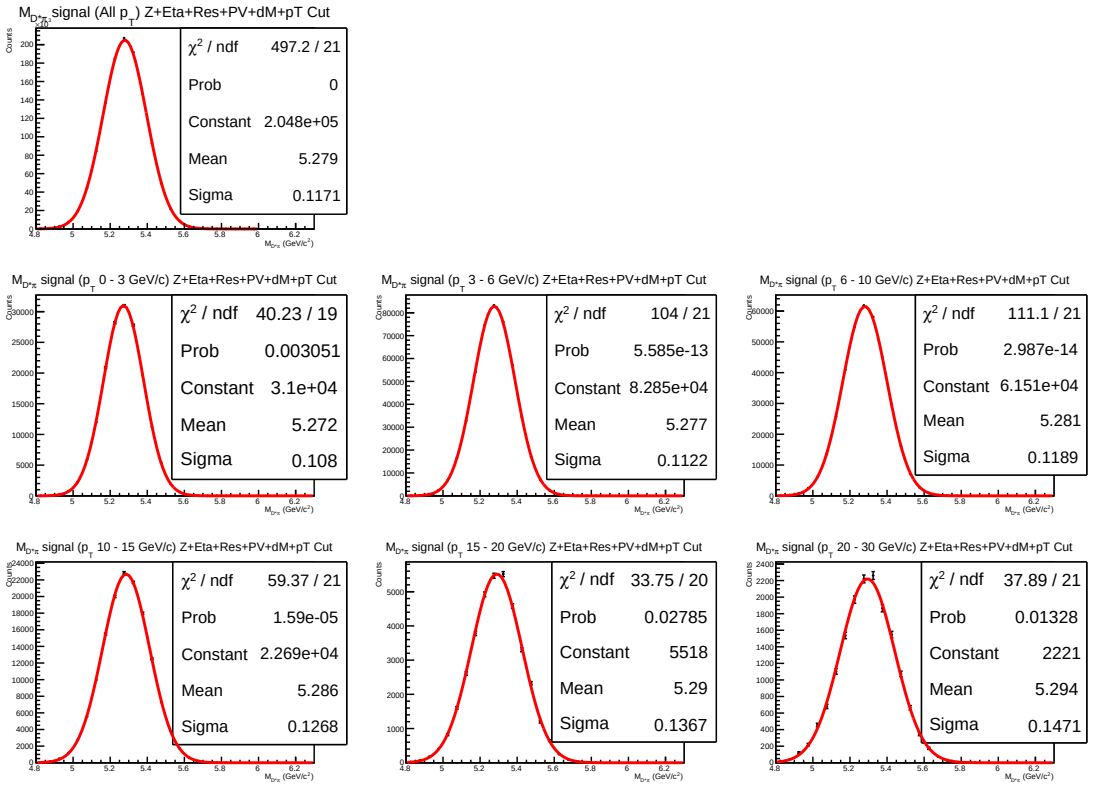

FIGURE A.1: Invariant mass distribution of $D^*\pi$ pairs. First plot is the p_T integrated case, the other six plots are for the different transverse momentum intervals (0 - 3, 3 - 6, 6 - 10, 10 - 15, 15 - 20 and 20 - 30 GeV/c).

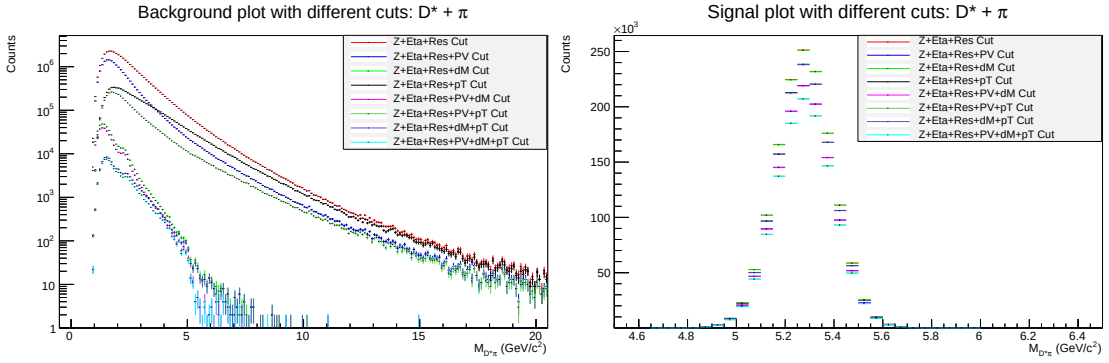

FIGURE A.2: The effect of the different cuts on the p_T integrated background (left) and signal (right) invariant mass plots for the investigated hadronic decay of a B^0 meson. The background decreases 99.77%, where only 17.06% of the signal entries are dropped by these selection cuts.

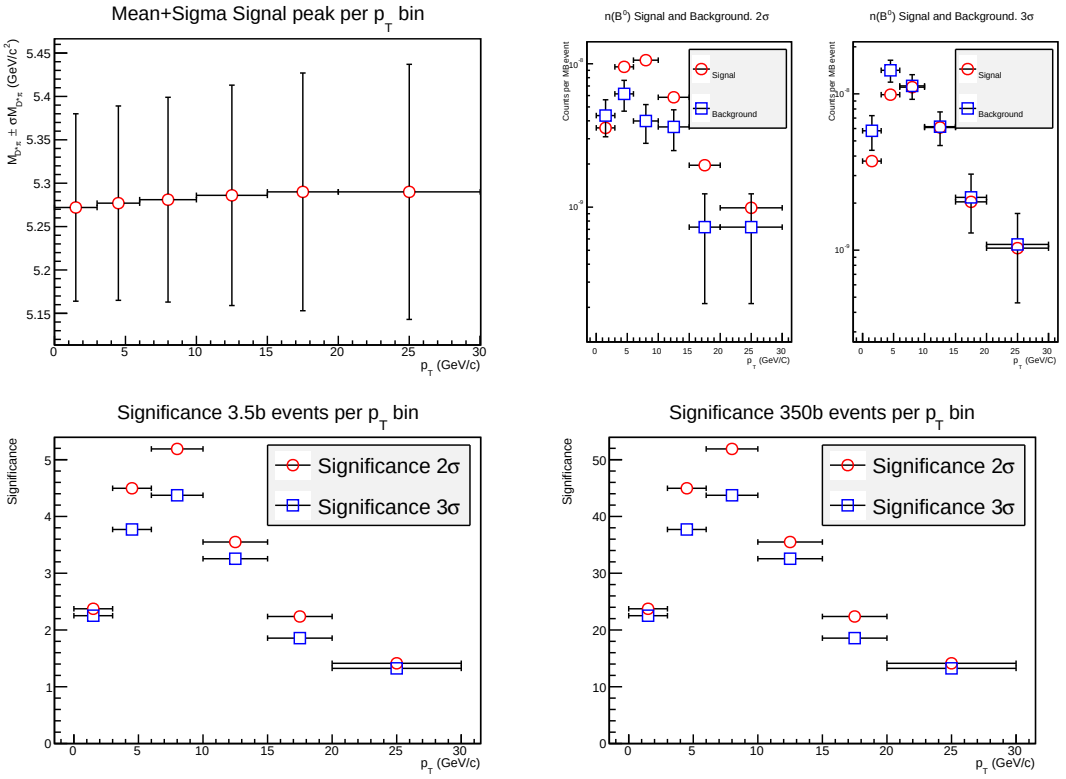

FIGURE A.3: Mean and width of the signal (upper left corner), counted number of S and B (upper right corner) and the statistical significance S_g for the six transverse momentum intervals for 3.5 (left) and 350 billion (right) $\sqrt{s} = 13$ TeV proton-proton collisions. Note that the error bars on the plot with the mean for the signal represent the sigma of the fit.

Appendix B

Results for the decay $B^0 \to D^{*+} + e^- + \bar{\nu_e}$ with p_T smearing only

The final results for the semi-leptonic decay of the B^0 meson studied in this thesis are presented in this chapter. These results are only transverse momentum smeared. This can be used as a comparison with the results presented in Chapter 5. The invariant mass distributions for the signal can be found in Figure B.1. The effect of the different selection cuts are specified in Figure B.2. In Figure B.4 the number of signal entries S, background entries B, signal-over-background ratio S/B and the statistical significance S_g are given. Unfortunately, the fluctuations in the combinatorial background were too large for the different p_T intervals, so the combined invariant mass spectra could not be fitted. Therefore these final results are calculated by the counting procedure. The fit on the p_T integrated invariant mass spectrum succeeded, which can be found in Figure B.3.

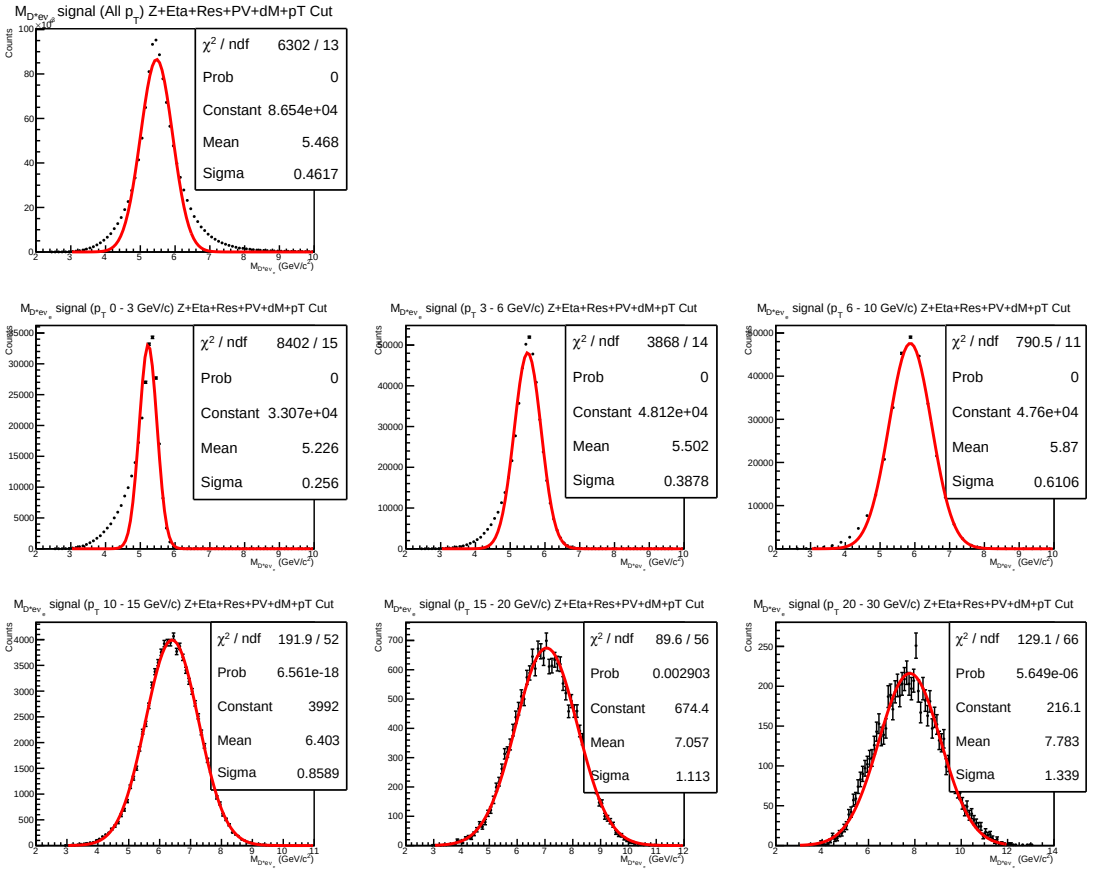

FIGURE B.1: Invariant mass distribution of D^*e pairs with a reconstructed ν_e. First plot is with p_T integrated, the other plots are for the six transverse momentum intervals (0 - 3, 3 - 6, 6 - 10, 10 - 15, 15 - 20, 20 - 30 GeV/c). Note the different ranges on the x axis.

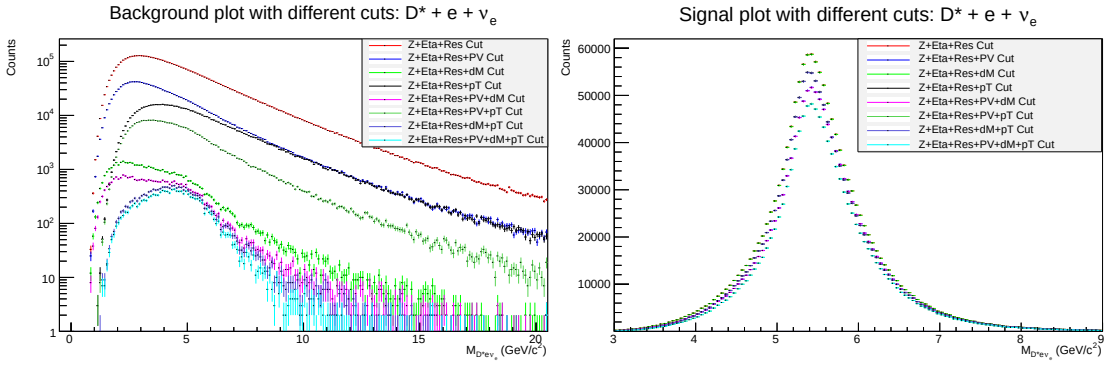

FIGURE B.2: The effect of the different cuts on the p_T integrated background (left) and signal (right) invariant mass plots for the investigated semi-leptonic decay of a B^0 meson. The background decreases 99.75 %, where only 18.90 % of the signal entries are dropped by these selection cuts.

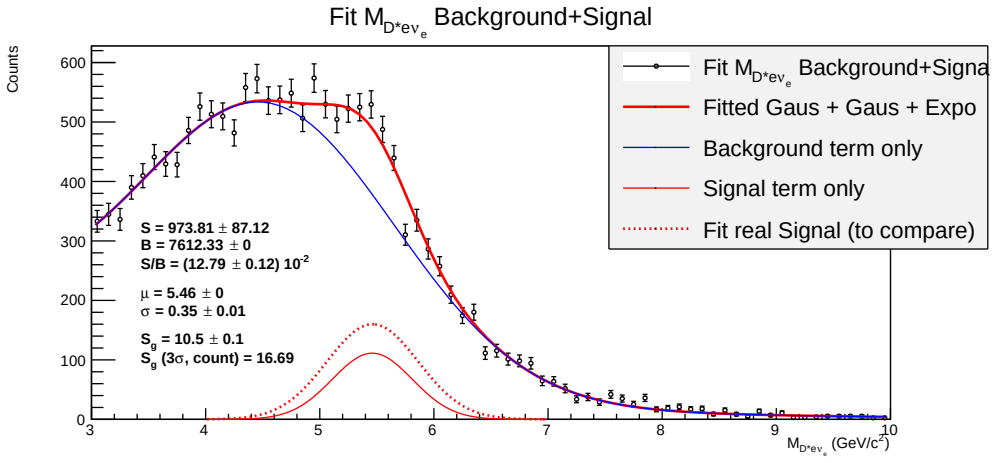

FIGURE B.3: Signal fitted on the combinatorial background for the p_T integrated invariant mass spectrum. S_g(count) is calculated with the counting procedure to check the result obtained with the fit.

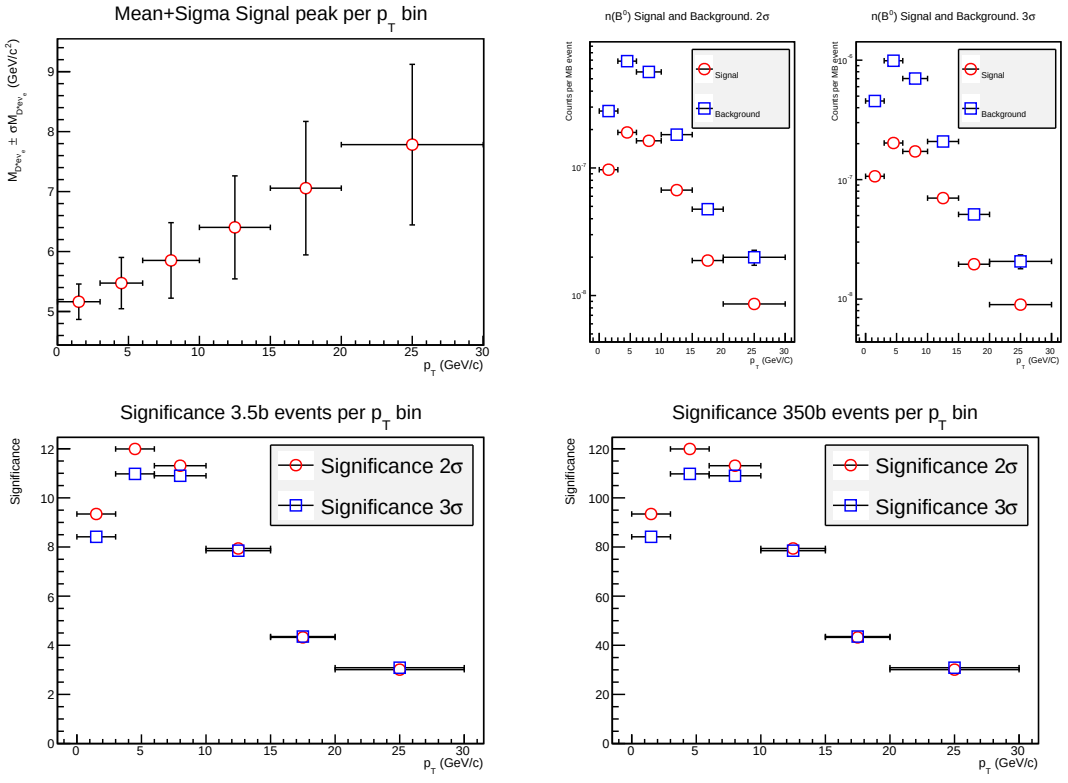

FIGURE B.4: Mean and width of the signal (upper left corner), counted number of S and B (upper right corner) and the statistical significance S_g for the six transverse momentum intervals for 3.5 (left) and 350 billion (right) proton-proton collisions at 13 TeV. Note that the error bars on the plot with the mean for the signal are the sigma of the fit.

Bibliography

[1] D. Leermakers, "Optimization of the reconstruction of $B^0 \to D^{*+}\pi^-$ and $D^{*+} \to D^0\pi^+$ decays with the ALICE detector", Bachelor's thesis, Utrecht University, 2014.

[2] K. Lessnoff, "A Study of the LHCb Experiments Sensitivity to CP Violation in Mixing and to Production Asymmetry in B_s Mesons, Using Semi-Leptonic Decays", PhD thesis, University of Bristol, 2009. LHCb-INT-2011-004.

[3] G. Aad *et al.*, (ATLAS Collaboration), "Observation of a new particle in the search for the Standard Model Higgs boson with the ATLAS detector at the LHC", *Physics Letters B* 716 (2012) 1–29, [arXiv:1207.7214].

[4] V. Barnes *et al.*, "Observation of a Hyperon with Strangeness Minus Three", *Phys. Rev. Lett.* 12 (1964) 204–206.

[5] F. Abe and others, (CDF Collaboration), "Observation of Top Quark Production in $\overline{p}p$ Collisions with the Collider Detector at Fermilab", *Phys. Rev. Lett.* 74 (1995) 2626–2631, [arXiv:hep-ex/9503002].

[6] A. O. Sushkov, W. J. Kim, D. A. R. Dalvit, and S. K. Lamoreaux, "New experimental limits on non-newtonian forces in the micrometer range", *Phys. Rev. Lett.* 107 (2011) 171101, [arXiv:1108.2547].

[7] P. MissMJ, "Standard Model of Elementary Particles". http://upload.wikimedia.org/wikipedia/commons/0/00/Standard_Model_of_Elementary_Particles.svg. November 15, 2014.

[8] Y. Hsiao and C. Geng, "Identifying glueball at 3.02 GeV in baryonic B decays", *Physics Letters B* 727 (2013) 168–171, [arXiv:1302.3331].

[9] C. Bal, "Elementary Particles". http://www.zamandayolculuk.com/cetinbal/elementaryparticles.htm. November 22, 2014.

[10] (Brookhaven National Laboratory), "Closing in on the Border Between Primordial Plasma and Ordinary Matter". http://www.bnl.gov/rhic/news2/news.asp?a=1446&t=pr. November 18, 2014.

[11] S. R. Soltz, "A question of quarks". https://str.llnl.gov/str/JanFeb03/Soltz.html. November 22, 2014.

[12] M. Djordjevic and M. Gyulassy, "Where is the charm quark energy loss at RHIC?", *Physics Letters B* 560 (2003) 37–43, [arXiv:nucl-th/0302069].

[13] (ALICE Collaboration), "The ALICE experiment". http://aliceinfo.cern.ch/Public/en/Chapter2/Chap2Experiment-en.html. November 19, 2014.

[14] K. Aamodt and others, (ALICE Collaboration), "Alignment of the ALICE Inner Tracking System with cosmic-ray tracks", *Journal of Instrumentation* 5 (2010) [arXiv:1001.0502].

[15] B. Abelev and Others, (ALICE Collaboration), "Technical Design Report for the Upgrade of the ALICE Inner Tracking", *Journal of Physics G: Nuclear and Particle Physics* 41 (2014).

[16] (ALICE Collaboration), "The ALICE Time Projection Chamber (TPC)". http://aliceinfo.cern.ch/Public/en/Chapter2/Chap2_TPC.html. November 26, 2014.

[17] P. Christiansen, (ALICE Collaboration), "High identified particle production in ALICE", *Nuclear Physics A* 910-911 (2013) 20–26, [arXiv:1208.5368].

[18] (ALICE Collaboration), "The ALICE Time of Flight Detector". http://aliceinfo.cern.ch/Public/en/Chapter2/Chap2_TOF.html. November 26, 2014.

[19] C. Lippmann, "Particle identification in ALICE: an extra boost in QGP studies - Part B". http://alicematters.web.cern.ch/?q=CL_PID2. January 9, 2015.

[20] R. Brun and F. Rademakers, "ROOT - An object oriented data analysis framework", *Nuclear Instruments and Methods in Physics Research* 389 (1997) 81–86.

[21] T. Sjöstrand *et al.*, "A brief introduction to PYTHIA 8.1", *Computer Physics Communications* 178 (2008) 852–867, [arXiv:0710.3820].

[22] S. Agostinelli *et al.*, "Geant4 - a simulation toolkit", *Nuclear Instruments and Methods in Physics Research* 506 (2003) 250–303.

[23] (ALICE Collaboration), "AliRoot Documentation". http://aliceinfo.cern.ch/Offline/AliRoot/Manual.html. November 22, 2014.

[24] (CERN), "WLCG Worldwide LHC Computing Grid". http://wlcg-public.web.cern.ch/. November 25, 2014.

[25] K. Olive *et al.*, (Particle Data Group Collaboration), "The Review of Particle Physics", *Chinese Physics C* 38 (2014).

[26] T. Sjöstrand *et al.*, "PYTHIA 6.4 physics and manual", *Journal of High Energy Physics* 2006 (2006) [arXiv:hep-ph/0603175].

[27] M. Cacciari *et al.*, "The p_T spectrum in heavy-flavour hadroproduction", *Journal of High Energy Physics* 1998 (1998) [arXiv:hep-ph/9803400].

[28] M. Cacciari *et al.*, "Theoretical predictions for charm and bottom production at the LHC", *Journal of High Energy Physics* 2012 (2012) [arXiv:1205.6344].

[29] R. de Rooij, "Prompt d^{*+} production in proton-proton and lead-lead collisions, measured with the ALICE experiment at the CERN Large Hadron Collider", PhD thesis, Utrecht University, 2013.

[30] C. Ivan, "Open charm analysis with the ALICE detector in pp collisions at LHC", PhD thesis, Utrecht University, 2010.

[31] B. Abelev *et al.*, "Measurement of charm production at central rapidity in proton-proton collisions at $\sqrt{s} = 7$ tev", *Journal of High Energy Physics* 2012 (2012) [arXiv:1111.1553].